Gastroenterology 2025;■:1–15

Therapeutic Targeting of Oncogene-induced Transcription-Replication Conflicts in Pancreatic Ductal Adenocarcinoma

Shanna J. Smith,[1] Fan Meng,[2] Robert G. Lingeman,[1] Caroline M. Li,[1] Min Li,[3] Galyah Boneh,[2] Toni T. Seppälä,[4,5] Thuy Phan,[2] Haiqing Li,[6] Richard A. Burkhart,[4] Vishwas Parekh,[7] Syed Rahmanuddin,[8] Laleh G. Melstrom,[2] Robert J. Hickey,[9] Vincent Chung,[10] Yilun Liu,[3] Linda H. Malkas,[1] and Mustafa Raoof[2,3]

[1]Department of Molecular Diagnostics and Experimental Therapeutics, Beckman Research Institute of City of Hope, Duarte, California; [2]Department of Surgery, City of Hope Cancer Center, Duarte, California; [3]Department of Cancer Genetics and Epigenetics, City of Hope Cancer Center, Duarte, California; [4]Division of Hepatobiliary and Pancreatic Surgery, Johns Hopkins University School of Medicine, Baltimore, Maryland; [5]Department of Gastroenterology and Alimentary Tract Surgery and TAYS Cancer Centre, Tampere University Hospital, Tampere, Finland; [6]Integrative Genomic Core, Beckman Research Institute of City of Hope, Duarte, California; [7]Department of Pathology, City of Hope Cancer Center, Duarte, California; [8]Department of Radiology, City of Hope Cancer Center, Duarte, California; [9]Department of Cancer Biology and Molecular Medicine, Beckman Research Institute of City of Hope, Duarte, California; and [10]Department of Medical Oncology, City of Hope Cancer Center, Duarte, California

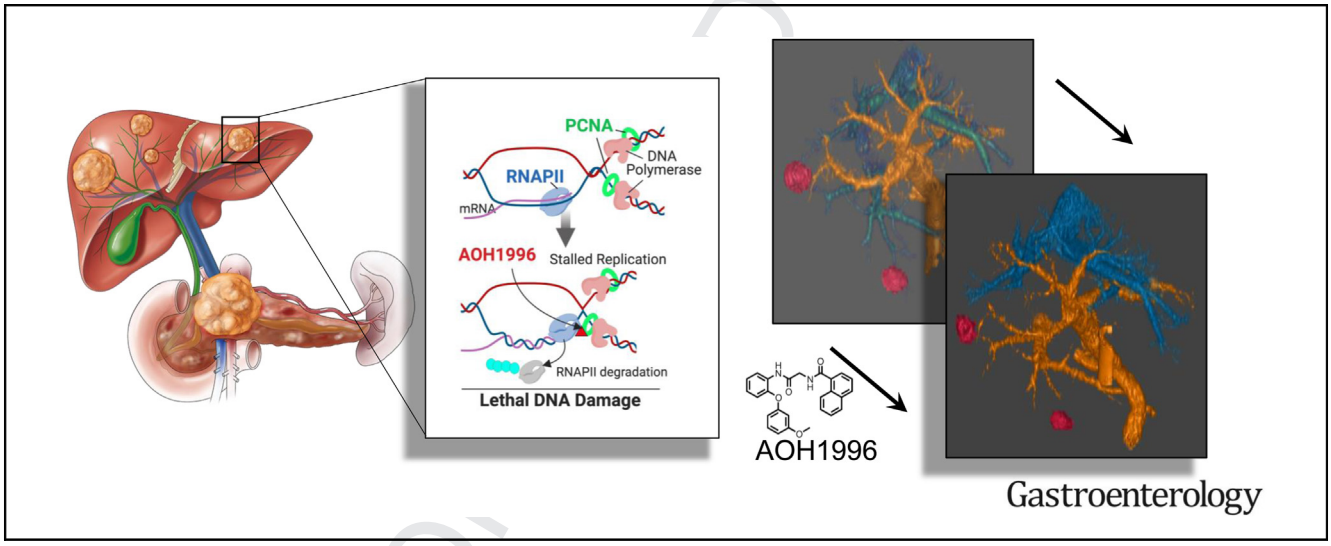

BACKGROUND AND AIMS: Transcription-replication conflicts (TRCs) are a key source of replication stress in cancer, with pancreatic ductal adenocarcinoma (PDAC) showing uniquely high levels. This study investigated the mechanism, oncogene dependency, subtype specificity, and preclinical activity of the TRC-targeting molecule AOH1996 in PDAC models. Initial clinical evidence of AOH1996 activity in patients with PDAC is also provided. **METHODS:** The oncogene-dependent toxicity of AOH1996 was studied in KRAS(G12D)-inducible systems. Its effects on replication fork progression, TRCs, DNA damage, cell cycle, and apoptosis were assessed in PDAC cell lines. Subtype-specific responses were tested in organoids, and in vivo efficacy was evaluated using murine and patient-derived xenografts. Clinical activity was measured through radiographic response and progression-free survival in patients. **RESULTS:** AOH1996 exhibited dose-dependent cytotoxicity reliant on KRAS(G12D) induction (average half maximal inhibitory concentration: 0.93 μM). It inhibited replication fork progression and induced TRCs by enhancing interactions between RNA Polymerase II and proliferating cell nuclear antigen, causing transcription-dependent DNA damage and transcription shutdown. Organoids with high replication stress were most sensitive (half maximal inhibitory concentration: 406 nM–2 μM). In mouse models, AOH1996 reduced tumor growth, induced tumor-selective DNA damage, and prolonged survival (median 14 vs 21 days, $P = .04$) without toxicity. Two patients with chemotherapy-refractory PDAC treated with AOH1996 showed up to 49% tumor shrinkage in hepatic metastases. **CONCLUSIONS:** AOH1996 safely and effectively targets TRCs in preclinical PDAC models, with initial clinical evidence supporting its potential for treating chemotherapy-refractory PDAC. Further clinical development is warranted.

Keywords: Replication Stress; AOH1996; PCNA Inhibitor; DNA Damage; DNA Repair.

Genomic instability in cancers is a direct consequence of DNA damage from both endogenous and exogenous insults.[1] Replication stress from oncogenes, such as KRAS and MYC in pancreatic ductal adenocarcinoma (PDAC), is a major source of endogenous insult on the DNA. For instance, oncogenic KRAS is a pathognomonic feature of PDAC, occurring in 95% of patients.[2] KRAS and other oncogenes place significant demands on the DNA replication machinery, leading to unrectified errors and genome instability.[3] The oncogene–replication stress–genomic instability axis is now a well-accepted hallmark of oncogene-driven cancers such as PDAC.[4]

Oncogenic mutations in PDAC induce DNA damage through reactive oxygen species and hyper-replication.[5] Emerging studies have highlighted hyper-transcription as another major impeding replication fork progression, resulting in DNA damage.[3,6,7] To counteract such DNA damage, KRAS-driven PDAC cells activate DNA damage response pathways such as ATR-Chk1 for DNA repair and TP53 co-mutations enable DNA damage tolerance despite replication stress.

Targeting of adaptive DNA repair pathways in PDAC is an attractive therapeutic strategy, but early attempts (eg, Chk1 inhibition) were met with disappointing results in the clinic.[8] However, Food and Drug Administration approval of poly(adenosine diphosphate–ribose) polymerase (PARP) inhibitors marks a breakthrough for tumors with homologous recombination (HR) repair deficiencies.[9] BRCA-related HR mutations occur in 4% to 7% of PDAC cases,[10] and PARP inhibitors significantly extend progression-free survival in these patients (7.4 vs 3.8 months, hazard ratio 0.53; $P = .004$).[11,12] This trial validates the utility of DNA-damaging therapies to improve outcomes in PDAC.[13]

Most patients with PDAC lack HR deficiency, necessitating new approaches for cancer-specific DNA damage. Transcriptomic analyses classify PDAC into classical and basal subtypes, the latter linked to therapy resistance and worse survival. A deeper analysis of the transcriptomic subtypes demonstrates that the genes associated with replication stress are enriched in the basal subtype.[14] This high replication stress phenotype is distinct from a previously recognized DNA repair deficiency phenotype and may represent a novel therapeutic vulnerability.

We evaluated targeting replication stress in PDAC using AOH1996, a bioavailable proliferating cell nuclear antigen (PCNA) inhibitor.[15] PCNA, a highly conserved "ringmaster" of the genome, forms a homotrimer processivity clamp encircling DNA: this orientation with respect to the DNA allows PCNA to act as a scaffold for binding of key proteins during DNA replication and repair.[16] Cancer cells critically depend on PCNA, as evidenced by its high expression in PDAC and its association with tumor aggressiveness and metastasis.[17,18]

Earlier concerns about PCNA inhibitor toxicity limited progress.[19] The development of cancer-selective, nontoxic AOH1996 enables targeting replication stress high PDAC.[15] This study investigated its mechanism, subtype specificity, and preclinical efficacy across cell lines, organoids, and murine models. We also report the first clinical evidence of AOH1996 activity in patients with PDAC, forming a basis for future clinical trials targeting replication stress in PDAC.

WHAT YOU NEED TO KNOW

BACKGROUND AND CONTEXT

The need to deal with transcription-dependent replication stress is a unique dependency in pancreatic cancer. Whether this can be targeted for therapeutic purposes in preclinical models and patients remains unknown.

NEW FINDINGS

This is the first-ever preclinical and clinical study of therapeutic targeting of transcription-replication conflicts in pancreatic cancer using a novel small molecule.

LIMITATIONS

To realize the full potential of therapeutic targeting of transcription-replication conflicts, larger clinical and biomarker discovery studies are needed.

CLINICAL RESEARCH RELEVANCE

Pancreatic cancer is a lethal disease with few treatment options. The mechanistic, preclinical, and clinical evidence presented here demonstrates a new strategy to target pancreatic cancer.

BASIC RESEARCH RELEVANCE

The study provides a strong rationale for further research in delineating transcription-replication conflict resolution mechanisms in pancreatic cancer.

Methods

Materials

AOH1996 was a generous gift from Dr Long Gu and Dr Linda Malkas and was synthesized and isolated to >95% purity in house by the Chemical GMP Synthesis Facility at City of Hope Comprehensive Cancer Center. Compound was received in powder form and stored at −20°C. Before use, for in vitro experiments, AOH1996 was dissolved in sterile DMSO (Fisher Scientific) to a concentration of 20 mM, and aliquots were stored at −20°C.

Abbreviations used in this paper: **ANOVA, analysis of variance; CT, computed tomography; DMSO, dimethyl sulfoxide; DRB, 5,6-dichloro-1-beta-D-ribofuranosylbenzimidazole; HPNE, human pancreatic ductal-derived cell line; HR, homologous recombination; IC50, half maximal inhibitory concentration; PCNA, proliferating cell nuclear antigen; PDAC, pancreatic ductal adenocarcinoma; PLA, proximity ligation assay; TRC, transcription-replication conflict; TUNEL, terminal deoxynucleotidyl transferase (TdT) dUTP nick-end labeling.**

0016-5085
https://doi.org/10.1053/j.gastro.2025.02.038

Cell Culture

All commercial cancer cell lines were cultured according to procedures established by the American Type Culture Collection (ATCC). HPNE E6/E7/st cells (ATCC, CR-4036) were transfected with doxycycline-inducible KRAS(G12D) expressing vector using viral transfection as described previously.[7] Patient-derived UPN3 cell line and KPC mouse-derived luciferase-expressing KPC cell line was a generous gift from Dr Edward Manuel (City of Hope). Luciferase expression in KPC cell line was achieved using lentiviral transduction (Invitrogen).[20] iKRAS and KPCXY cells were a generous gift from Dr Haoqiang Ying[21] and Dr Ravikanth Maddipati.[22] Culture conditions are listed in the Supplementary Methods.

In Vitro Cytotoxicity of AOH 1996

Exponentially growing (1×10^3 to 5×10^3, depending on cell doubling time) pancreatic cancer cells (lines described previously) were seeded in 96-well plates. In (at least) quadruplicate, increasing concentrations of AOH1996 were added to each well and incubated for 48 hours at 37°C in 5% CO_2. Organoid experiments were performed in 384-well plates using a high-throughput protocol described previously.[23] Organoids were exposed to control conditions or AOH1996 for 72 hours. Cell viability was determined using the CellTiter-Glo Luminescent Cell Viability Assay (Promega), according to the manufacturer's instructions. Activity was calculated as percentage of cells alive/concentration vs control cells with no AOH1996 treatment, where 100% indicates no cell death (high ATP levels) and 0% indicates complete cell death (low or no ATP levels). Data were analyzed and IC50 values were determined following the guidelines described by Sebaugh[24] using the sigmoidal dose-response equation in GraphPad Prism 5 software.

DNA Fiber Analysis

DNA fiber assays were performed using a modified version of the standard technique described by Frum et al,[25] as detailed in the Supplementary Methods.

Western Blot Analysis

Western blot analysis was performed using standard methods as previously described and noted in the Supplementary Methods.[17]

Immunocytochemistry Staining of gH2AX and Confocal Imaging

Immunocytochemistry was performed as described previously[26] using standard protocol. For confocal imaging, a Zeiss LSM 700 Confocal Microscope was used. Images were acquired using an LCI Plan Neofluar 63x/1.3 Water Imm Corr M27 objective for a 1024 × 1024-pixel array at 0.05 microns/pixel (see Supplementary Information for details).

Cell Proliferation and Apoptosis Assays

Flow cytometric cell proliferation assay was performed using BD Pharmingen BrdU Flow Kit (BD Life Sciences) according to the manufacturer's instructions. Cell proliferation with real-time cell analysis assay was performed using E-plate (Agilent 05469830001) per the manufacturer's instructions. Nuclear apoptosis was assessed by the terminal deoxynucleotidyl transferase (TdT) dUTP nick-end labeling (TUNEL) assay using the In Situ Cell Death Detection Kit, TMR red kit (Roche) according to the manufacturer's protocol (see the Supplementary Information for details).

PLA for TRC and Global RNA Transcription Quantification

To quantify TRCs, we performed PLA to measure the foci with RNAPII-CTD-S2 and PCNA proximity as described previously.[7] Global RNA quantification was performed using the Click-iT RNA Alexa Fluor488 Imaging Kit (Thermo Fisher Scientific) according to manufacturer supplied methodology.[27]

RNA-Sequencing Analysis

RNA sequencing was performed as described previously.[23] The RNA-sequencing datasets are merged based on the Hg38 gene symbols.

Mouse Models of Pancreatic Cancer

Orthotopic syngeneic and ectopic patient-derived xenograft PDAC models were generated as described previously.[20,28] On engraftment, mice were then randomized to AOH1996 or excipient groups. All animals were handled, housed, and studied in accordance with a protocol (Institutional Animal Care and Use Committee #18026) that was reviewed and approved by the City of Hope Institutional Animal Care and Use Committee. Immunohistochemistry and TUNEL assays on mouse tissues were performed using standard methods (see the Supplementary Methods for details).

Human Studies

The patient treated with AOH1996 was enrolled under City of Hope Institutional Review Board 21310 (NCT05227326) after informed consent. Contrast CT of the chest, abdomen, and pelvis performed from the lung apices through the pelvis was obtained before and after treatment at 2-month intervals per protocol. Tumor volume measurements were derived from contrast CT reconstructions as detailed in the Supplementary Methods.

Statistical Analysis

Unless otherwise indicated, all statistical analyses were performed in Prism (version 10.30). When comparing a continuous variable between 2 groups, unpaired tests were used: unpaired *t* test for normally distributed data, and Mann-Whitney Rank test for skewed data. Welch's correction was applied when using unpaired *t* test if the variance was different between the groups being compared. When comparing a continuous variable across multiple groups (greater than 2), 1-way analysis of variance (ANOVA) was used. To account for multiple comparisons to the control condition, Dunnet multiple comparison test was used. When comparing all the groups with each other, Tukey multiple comparison test was used. Sidak multiple comparison test was used to compare a set of independent comparisons. For dose-response analyses, we used the nonlinear regression (log-inhibitor vs response – standard slope) to fit the viability data generated from the CellTiter-Glo experiments. To compare IC50 values, we asked if the best-fit

values of IC50 defer between cell lines. Pairwise comparison of IC50 values was performed using extra sum-of-squares F-test. For survival analysis, Kaplan Meir plots are shown, and log-rank test was performed to evaluate equality of survival functions.

Results

AOH1996 Causes Oncogene-Dependent Toxicity

We assessed the impact of AOH1996 on replication stress in PDAC using a telomerase-immortalized human pancreatic ductal-derived (HPNE) cell line with doxycycline-inducible KRAS(G12D).[29] On doxycycline induction, this system induces replication stress, R-loops, transcription-replication conflicts (TRCs), and DNA damage.[7] Exposing these cells to AOH1996 or dimethyl sulfoxide (DMSO) showed that AOH1996 selectively caused DNA damage, marked by γH2AX induction, in KRAS(G12D)-expressing cells but not in controls (Figure 1*A*)

To examine oncogene-dependent growth inhibition, we performed real-time cell assay that measures cell confluence/attachment over time. HPNE KRAS(G12D) cells were pre-induced for 72 hours with doxycycline or DMSO, then plated and allowed to grow for 40 hours followed by treatment with AOH1996 (7.8 nM). Doxycycline-induced HPNE cells treated with AOH1996 showed significant growth inhibition compared with uninduced cells, which proliferated normally (Figure 1*B*). For orthogonal validation of these findings, we used murine iKRAS cell lines (14837 and 14838), where KRAS(G12D) is expressed under doxycycline induction.[21] We observed that cells with KRAS(G12D) expression were highly sensitive to AOH1996, whereas KRAS(G12D)-extinct cells were resistant, as measured by CellTiter-Glo assay (Figure 1*C*).

Further, we tested AOH1996 across PDAC cell lines with various KRAS statuses (Panc1 – KRAS[G12D]; MIA Paca-2 – KRAS[G12C]; BxPC3 – KRAS[WT], BRAF [delL485-P490]; Capan1 – KRAS[G12V]; Murine, KPC – KRAS[G12D]) using CellTiter-Glo assay. The compound exhibited dose-dependent toxicity with half maximal inhibitory concentration (IC50) values ranging from 0.03 mM for BxPC3 cells to 2.5 mM for Panc1 cells (Average IC50 across cell lines 0.93 mM) (Figure 1*D* and *E*, Supplementary Figure 1*A*). Notably, BxPC3 cells are KRAS wild type, but they harbor a BRAF-activating 15–base pair deletion at L485-P490 that results in constitutive activation of MEK-ERK pathway and downstream oncogenic signaling like that seen with KRAS-activating mutations. The sensitivity of BxPC3 to AOH1996 suggests that the effect is not limited to mutant KRAS cell lines. BRCA2-mutant Capan-1 cells showed sensitivity like BRCA2-revertant and BRCA2-wild-type lines, indicating HR status had limited impact (Supplementary Figure 1).

Metastatic progression and replication stress in human PDAC is associated with upregulation of MYC signaling.[14,22] We performed additional experiments to determine if MYC overexpression could enhance the toxicity of AOH1996. To test this hypothesis, we used mouse cell lines isolated from KPCXY mice. Cell lines isolated from metastatic clones demonstrate a high MYC expression (and a basal transcriptomic signature) compared with those isolated from nonmetastatic clones, as previously shown.[22] The results now summarized in Figure 1*E* and *F* demonstrate that AOH1996 toxicity was significantly higher in metastatic clones (853-Y1-1, 471-R1-2, 832-CY10) compared with nonmetastatic clones (833-Y2, 471-CFP4, 852-RY4).

Together, these data demonstrate that AOH1996 causes oncogene-dependent growth inhibition and cytotoxicity independent of the oncogene driving replication stress.

AOH1996 Enhances Replication Stress and DNA Damage in PDAC Cells

To explore AOH1996-induced cytotoxicity mechanisms, we analyzed replication fork dynamics in MIA Paca-2 cells with intermediate sensitivity to AOH1996. AOH1996 caused dose-dependent replication fork stalling, with no significant increase in origin licensing as compensation (Figure 2*A–C*, Supplementary Figure 2*A* and *B*). Western blot and immunocytochemistry confirmed dose-dependent DNA damage (γH2AX induction) across cell lines (Figure 2*D* and *E*, Supplementary Figure 2*C*).

Flow cytometry showed robust late S and G2/M phase arrest in MIA Paca-2 cells treated with low-dose AOH1996, an effect amplified at higher doses (Figure 2*F* and *G*, Supplementary Figure 2*D*). TUNEL assays revealed dose-dependent apoptotic cell death (Figure 2*H* and *I*). These results demonstrate AOH1996 induces DNA damage, cell cycle arrest, and apoptosis.

Impact of AOH1996 on TRCs in PDAC

We have previously demonstrated that transcription-dependent replication stress through TRCs is a major mechanism of endogenous replication stress in human PDACs.[7] TRCs may therefore represent a unique targetable vulnerability in human PDAC. One of the proposed mechanisms of action of AOH1996 is the targeting of TRCs.[15] Specifically, AOH1996 promotes an interaction between RNA Polymerase II (APIM motif) and PCNA, potentially increasing TRCs. We examined the impact of AOH1996 on TRCs in Panc1 cells through a flow cytometry–based proximity ligation assay (PLA) and specifically measured foci with <40 nm proximity of RNAPII and PCNA.[7,30] At baseline, 50% of PDAC cells demonstrated high TRCs. On exposure to AOH1996 for 24 hours, this proportion increased to 65% to 82% depending on the dose of AOH1996 (Figure 3*A* and *B*). Similarly, immunocytochemistry-based RNAPII-PCNA PLA[7] demonstrated dose-dependent increase in TRCs on AOH1996 exposure for 24 hours (Figure 3*C*).

We then asked if the DNA damage induced by AOH1996 is in part explained by AOH1996-induced increase in TRCs. The exponentially growing MIA Paca-2 cell culture was exposed to AOH1996, with or without a transcription inhibitor—DRB (5,6-dichloro-1-beta-D-ribofuranosylbenzimidazole)—and DNA damage was measured by g-H2AX immunocytochemistry (Figure 3*D*). The results were compared with DMSO control, gemcitabine treatment, or a combination of gemcitabine and DRB treatment. Gemcitabine, a DNA-damaging nucleoside analogue approved by the

Food and Drug Administration for patients with pancreatic cancer, causes transcription-independent DNA damage by stalling of replication forks. The results demonstrate that both AOH1996 and gemcitabine caused DNA damage. But, contrary to gemcitabine, AOH1996-induced DNA damage was significantly inhibited by DRB (81% vs 31%, $P = .0005$), suggesting that AOH1996-induced DNA damage is at least partially transcription-dependent. To determine if AOH1996-related DNA damage is preferentially localized to the nucleolus, we repeated the experiment and quantified the colocalization of nucleolar marker—nucleolin with gH2AX. Our results indicate that DNA damage marker

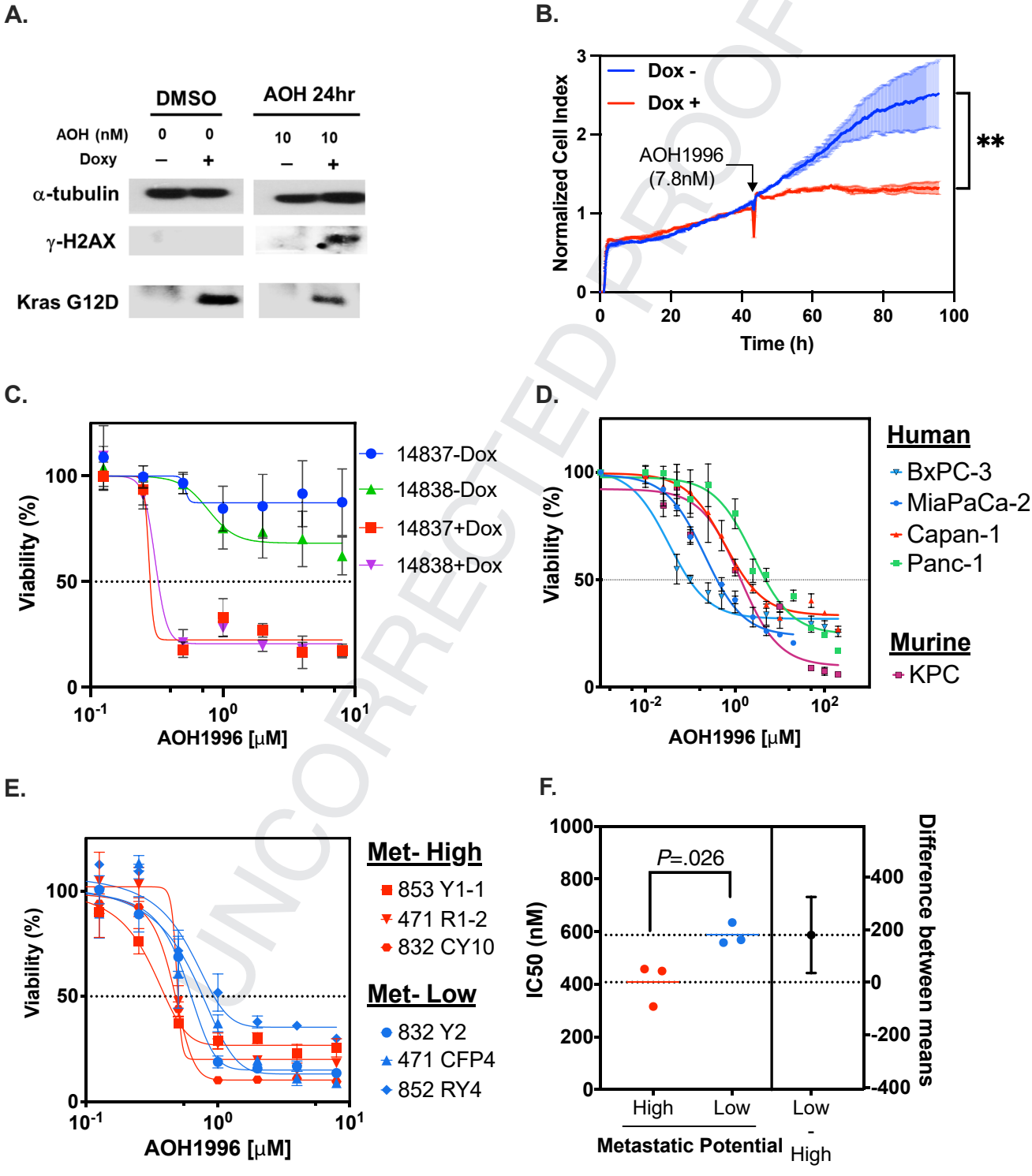

(gH2AX) does not colocalize with nucleolin in cells treated with AOH1996. However, in gemcitabine-treated cells there was a weak but significant colocalization (Pearson Coefficient 0.15, $P < .0001$, Supplementary Figure 3*A*), suggesting a slight preference for nucleolar regions with gemcitabine-induced DNA damage.

Prior work has demonstrated that persistent TRCs ultimately result in RNAPII degradation to resolve replication stress.[31,32] To test this possibility, we evaluated the effects of AOH1996 on RNAPII expression using western blot analysis in pancreatic cancer whole-cell lysates (using anti-RNAPII A10 antibody). Our results (Figure 3*E*) indicate that AOH1996 (500 nM for 12 hours) caused preferential degradation of the active RNAPII–RNAPIIo (as opposed to inactive RNAPII–RNAPIIa), which could be inhibited by the proteasome inhibitor, MG132; like the UV exposure (positive control). Notably, gemcitabine caused minimal to no change in active RNAPII (Supplementary Figure 3*B*). Additional experiments demonstrated that AOH1996 also caused proteasome-dependent degradation of RNAPI in MIA Paca-2 cells but not in Panc1 cells, whereas RNAPIII levels were unaffected by AOH1996. We then asked if degradation of RNAPII and RNAPI would impact overall transcription in MIA Paca-2 cells. As shown in Figure 3*F* and *G*, MIA Paca-2 cells exposed to AOH1996 (500 nM, 12 hours) demonstrated a significant decrease in global RNA synthesis compared with DMSO control, as measured by 5-ethynyl uridine incorporation assay. Transcription inhibitor, DRB, was used as a positive control. Gemcitabine had a very small but significant effect on RNA synthesis. Collectively, the results from these experiments provide evidence of TRC-dependent DNA damage and transcription shutdown in PDAC cells from treatment with AOH1996.

AOH1996 Targets Replication Stress High Subtype of PDAC

AOH1996 demonstrated robust activity in all organoid lines tested with varying potency (IC50 406 nM–2 mM) as shown in Figure 4*A* and Supplementary Figure 4. Principal component analysis plot (Figure 4*B*) and gene-expression heatmap demonstrate that sensitive and resistant lines cluster separately based on gene-expression profiles with 43 downregulated genes and 87 upregulated genes in sensitive organoids compared with resistant organoids (Figure 4*C*). Distinct clustering of resistant and sensitive organoid lines based on gene-expression analysis suggests that transcriptomic profiles of PDAC predicts sensitivity to AOH1996.

Organoid lines were therefore annotated as classical, basal, both, or none based on their gene-expression profiles as previously described.[33] SU2C-AJ was strongly basal, whereas JHH-201 was weakly basal. JHH-224 and SU2C-043 demonstrated moderately classical profiles, whereas SU2C-052 was weakly classical. JHH162 demonstrated both basal and classical signatures, whereas SU2C-01 demonstrated neither (Figure 4*D*, Supplementary Figure 4). Two cell lines with a positive replication stress score were classified as replication stress high, SU2C-AJ (12.26) and JHH224 (3.14). AOH1996 was most potent in 2 of 3 cell lines with replication stress high transcriptomic signature (Figure 4*E*). One of these (SU2C-AJ) also had a strong basal signature, whereas the other 2 did not. Taken together, these data suggest that tumors with replication stress high transcriptomic signature may predict response to AOH1996, whereas the results with respect to basal vs classical signature are inconclusive.

In Vivo Therapeutic Efficacy of AOH1996 in PDAC

In a fast-growing orthotopic model of pancreatic cancer (average time from implantation to death ~4 weeks), AOH1996 reduced tumor size without significant toxicity to normal tissues (Figure 5*A–D*, Supplementary Figures 5 and 6). Tumor samples from the mice treated with AOH1996 had significantly higher proportions of nuclei with DNA damage (γH2AX) compared with control mice (mean 45.5% vs 11.8%, Nested *t* test, $P < .0001$, Figure 5*D*). There was a slight decrease in proliferation rate (measured by Ki67) and slight increase in apoptosis (measured by TUNEL assay), as shown in Supplementary Figure 7. These differences, however, were not statistically significant. We validated the results from this experiment and tested the efficacy of AOH1996 in a patient-derived xenograft model of PDAC, developed from a chemotherapy-refractory tumor with

Figure 1. AOH1996 causes oncogene-dependent toxicity. (*A*) Western blot analysis of HPNE cells with stable expression of doxycycline-inducible KRAS(G12D) vector. Cells were treated with/ without doxycycline to induce KRAS(G12D) expression for 48 hours and then treated with DMSO (control) or AOH1996 (10 nM) for another 24 hours. Representative western blot of the indicated proteins is shown from whole-cell lysates cells indicating induction of oncogenic KRAS and DNA damage (gH2AX) on KRAS induction, which is enhanced by AOH1996; a-tubulin is used as a loading control. (*B*) Real-time cell analysis of HPNE cells with stable expression of doxycycline-inducible KRAS(G12D) vector. Cells were grown with or without doxycycline and AOH1996 (7.8 nM) was added at the indicated time. Cell index was measured in real time. Cell index is a unitless measure of cellular impedance of electron flow caused by adherent cells depicting cell growth and confluence. Lines indicate average of 3 replicates and error bars indicate standard deviation. **Unpaired *t* test (with Welch's correction due to unequal variance) comparing cell index at 96-hour time point: $P = .009$. (*C–E*) Exponentially growing cells were exposed to increasing concentrations (0–20 μM) of AOH1996 for 48 hours and then analyzed using the CellTiter-Glo assay. Cell viability is reported as % of control, with 100% representing a zero response. Data points indicate mean, and error bars indicate standard deviation calculated from at least 3 to 8 replicates (see also Supplementary Figure 1*A* for IC50 comparison). (*F*) Estimation plot demonstrates difference in AOH1996 IC50 between metastatic and nonmetastatic cell lines from KPCXY mice. IC50 was calculated using a nonlinear variable slope (log)dose-response model as specified in Prism for each of the dose-response curves in (*D*). The difference between mean IC50 is depicted in black with error bars representing standard deviation. *P* value is calculated from an unpaired *t* test.

KRAS(G12V) and TP53 (p. Tyr205_Leu206delinsTer) commutation. AOH1996 significantly delayed the growth of the tumor, like in our previous results ($P = .013$, Figure 5*E*).

To measure the impact of AOH1996 on survival, we randomized mice with orthotopic KPC tumor to treatment with AOH1996 at 100 mg/kg or control (excipients only) 2 weeks

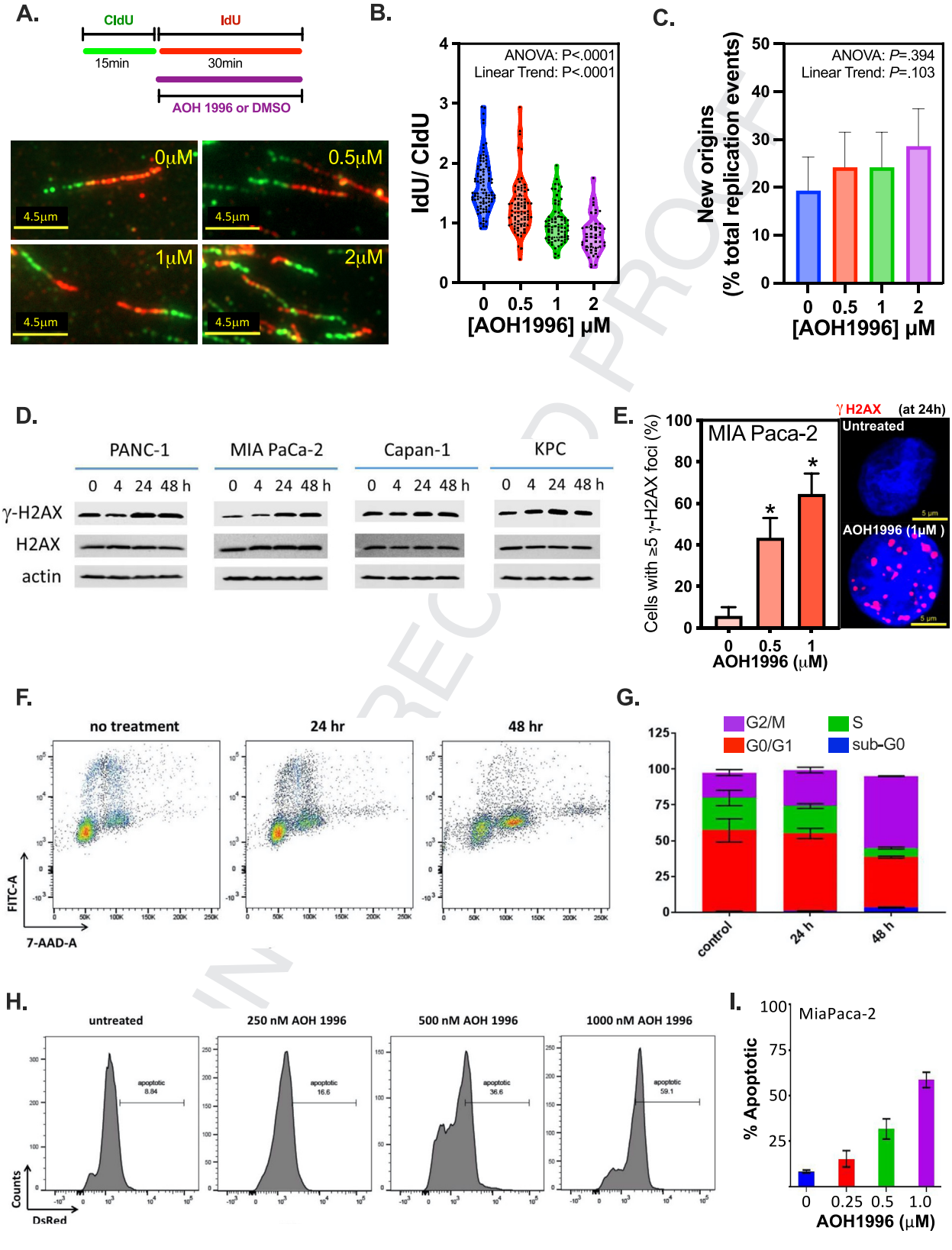

after orthotopic tumor implantation. Treatments were repeated daily (5 days/week) until the mice were moribund or met euthanasia criteria (Figure 5*F*). Mice treated with AOH1996 had significantly longer survival (median 21 days) than vehicle-treated controls (or "excipients," median 14 days, $P = .04$). Mice in both groups had stable and similar weights during treatment (Figure 5*G*, Supplementary Figure 8). Collectively, these studies provide evidence of preclinical efficacy and safety of TRC targeting using AOH1996 in PDAC.

First Evidence of AOH1996 Efficacy in Human Metastatic PDAC

Given the promising preclinical activity, a phase 1 clinical trial (NCT05227326) was initiated with the primary goal of identifying maximum tolerated dose and dose-limiting toxicity of AOH1996 in patients with refractory solid tumors. The first patient with PDAC enrolled on the trial derived clinical benefit from AOH1996. The patient presented with obstructive jaundice secondary to a mass in the head of the pancreas that was biopsy confirmed to be PDAC. The staging workup demonstrated metastases in the retroperitoneal lymph nodes and lungs. Genomic profiling demonstrated several mutations: KRAS(G12R), ARID1A (R1722*), and TP53 (S241F). The tumor was microsatellite stable, and tumor mutation burden was low. Germline testing was negative for pathogenic mutations. The patient was initiated on gemcitabine and nab-paclitaxel, to which there was stabilization of disease lasting 9 months. Subsequently, the patient was treated with 5-fluorouracil, leucovorin, and liposomal irinotecan (FOLFIRINOX) and developed rapidly progressive disease within 3 months. The patient also developed 2 new liver metastases at this time. The patient was then enrolled on the phase 1 clinical trial and was treated with single-agent AOH1996 (dose level: 240 mg twice daily). After 2 months of therapy, the patient demonstrated stable disease in retroperitoneal lymph nodes and the primary tumor. Notably, there was approximately 49% tumor shrinkage in both hepatic metastases (Figure 6*A* and *B*). However, there was slight growth of innumerable sub-cm lung metastases. Overall, the patient was deemed to have stable disease by RECIST (Response Evaluation Criteria in Solid Tumors) version 1.1. The patient continued AOH1996 for another 2 months, after which they demonstrated disease progression at all tumor sites and a rise in tumor marker CA 19-9 from 58 U/mL (pretreatment) to 68 U/mL (posttreatment). Overall, this resulted in a progression-free survival of 4 months on AOH1996.

A second consecutive patient with chemorefractory PDAC was subsequently enrolled on the trial. Genomic profiling demonstrated the following mutations: KRAS (G12D), CDKN2A, TP53 (R273H). The tumor was microsatellite stable and tumor mutation burden was low. The patient presented with a pancreatic uncinate tumor with vascular involvement. After 2 months of FOLFIRINOX, the patient developed local progression as well as distant (hepatic) metastasis. The patient was treated with second-line gemcitabine and nab-paclitaxel to which there was favorable response for 8 months, subsequently followed by progression as evidenced by multiple lung metastases and growth in a solitary liver metastasis and primary tumor. After 1 month of AOH1996 monotherapy (dose level: 480 mg twice daily), the patient developed obstructive jaundice and was re-imaged. Computed tomography (CT) scan demonstrated a 43% tumor shrinkage in the solitary hepatic metastasis (Figure 6*A* and *B*); however, the patient developed peritoneal metastases. The primary tumor was stable in size, and the lung metastases showed mild progression.

These 2 cases highlight proof-of-concept clinical activity of AOH1996 in patients with chemotherapy-refractory PDAC with clinical benefit in 1 patient.

Discussion

Genome instability in PDAC results from endogenous and exogenous DNA insults. Endogenous mechanisms, such

Figure 2. AOH1996 enhances replication stress and DNA damage in PDAC cells. (*A*) DNA fiber analysis was performed using exponentially growing MIA-Paca2 cells. Replicating DNA was labeled with chlorodeoxyuridine (CldU) for 15 minutes, followed by iododeoxyuridine (IdU) for 30 minutes. AOH1996 (indicated dose) or DMSO was added with IdU labeling. Representative images from 4 different conditions are shown. (*B*) Replication fork progression: IdU tract lengths were normalized to average chlorodeoxyuridine (CldU) length before drug treatment from the experiment shown in (*A*). Violin plots are shown. One-way ANOVA demonstrated significant differences between the groups ($P < .0001$). There was linear trend with increasing dose of AOH1996 (Slope -0.29, $P < .0001$) (see Supplementary Figure 2*A* and *B* for replication speed before and after drug treatment). (*C*) New origins: IdU tracts without preceding CldU tracts were counted and expressed as a proportion of total replication forks (CldU and IdU) to calculate the number of new origins from the experiment shown in (*A*). Error bars represent 95% confidence interval encompassing proportion estimates. One-way ANOVA did not demonstrate any significant differences between treatments and there was a lack of linear trend, as shown. (*D*) Western blot: Pancreatic cancer cells were treated with 200 nM AOH1996 for increasing amounts of time (0–48 hours). Representative immunoblots of protein extracts from each cell line tested are shown. Actin was used as the loading control. (*E*) Immunocytochemistry for DNA damage marker (gH2AX) was performed in MIA Paca-2 cells exposed to increasing concentration of AOH1996 for 24 hours. There was a significant dose-dependent increase in the proportion of cells with DNA damage on AOH1996 treatment compared with controls. A representative experiment is shown. One-way ANOVA with Dunnett adjustment for multiple comparisons, $^*P < .0001$ relative to control. Error bars represent 95% confident intervals (also see Supplementary Figure 2*C*). (*F* and *G*) Flow cytometry (BrdU-FITC and 7-AAD) cell cycle analysis. MIA Paca-2 cells were treated with 200 nM of AOH1996 for 24 or 48 hours and then analyzed in triplicate. Average proportions are plotted in stacked bar graph with error bars indicating standard deviation. (Dose response is demonstrated in Supplementary Figure 2*D*). (*H* and *I*) MIA Paca-2 cells were treated with increasing concentrations of AOH1996 (0–1000 nM) for 24 hours. Apoptotic cells were labeled using TUNEL assay and quantified using flow cytometry in triplicate. Average proportions are plotted in bar graph with error bars indicating standard deviation.

as deficient DNA repair or oncogene-induced replication stress, are major contributors.[34] Although sporadic or germline DNA repair defects occur in up to 20% of patients with PDAC, replication stress driven by KRAS mutations is a hallmark, occurring in 95% of cases.[35] Oncogenes place significant demands on DNA replication and exacerbate

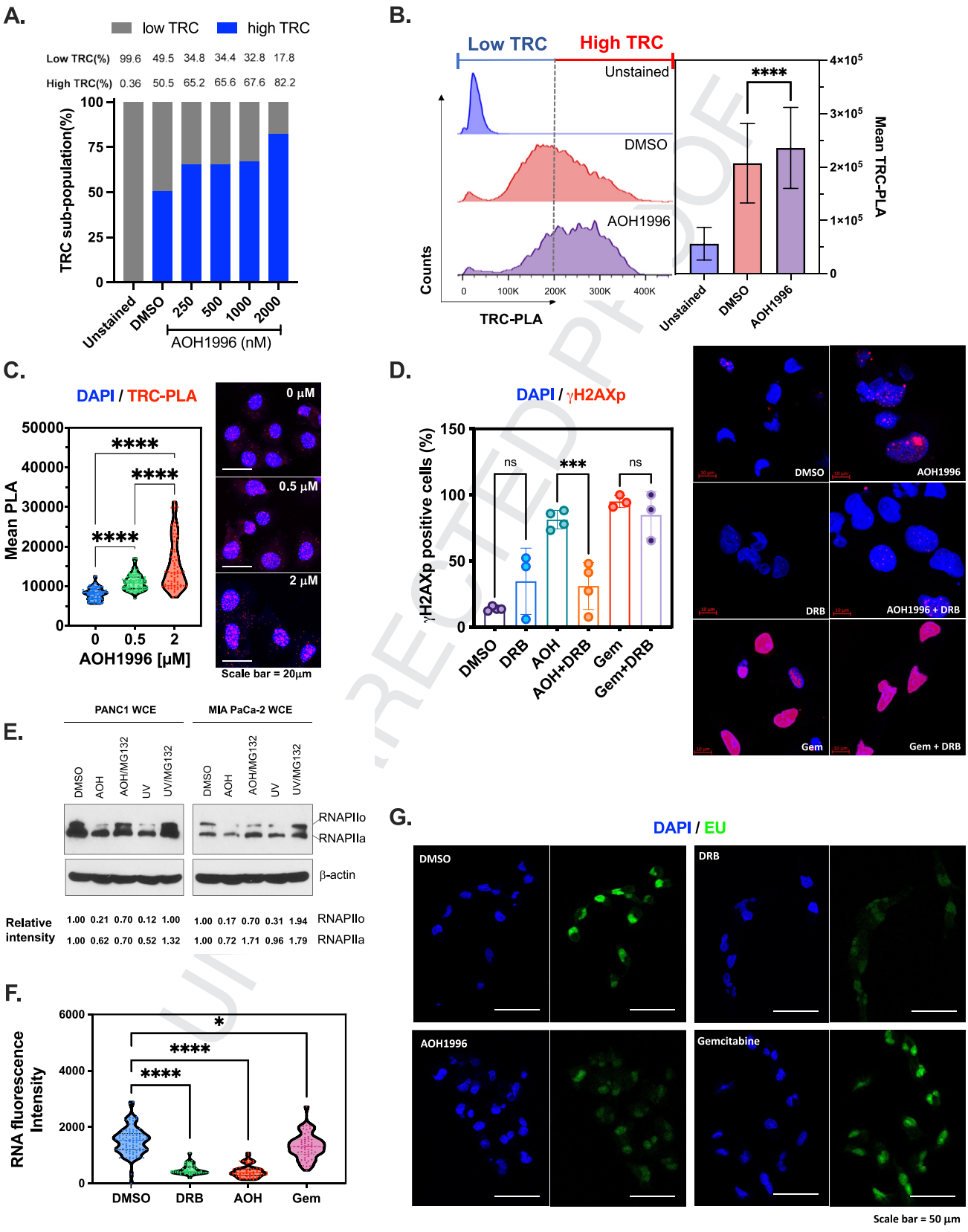

replication impediments, including transcription machinery, torsional stress, and non-B DNA structures.[32] Therefore, mechanisms enabling PDAC cells to replicate under these conditions present therapeutic opportunities.

Spatial and temporal deregulation of transcription and replication under oncogenic signaling increases TRCs.[3,36,37] This study provides the first evidence of targeting TRCs in PDAC using a small molecule inhibitor in preclinical models and patients with metastatic PDAC.

A growing body of literature provides preclinical evidence for TRC-targeting therapeutic approaches. For instance, Bowry et al[38] demonstrated that bromodomain and extra-terminal motif (BET) inhibitors (specifically BRD4 inhibition) may enhance TRCs through enhanced transcription of highly transcribed histone and other non–polyadenylated noncoding RNA genes. However, it remains to be defined if enhanced TRCs are related to the therapeutic effect of BET inhibitors.[38] Other strategies, such as Aurora A kinase inhibitors combined with ATR inhibitors, have shown success in neuroblastoma models by enhancing TRC-related DNA damage.[39] As another example, recently, MEPCE, a methylphosphate capping enzyme, was identified as a synthetic lethal interactor of BRCA1. Lack of MEPCE in a BRCA1-deficient context promoted RNAPII pausing, R-loops, TRCs, and TRC-related DNA damage and reduced growth of breast cancer xenografts.[40]

In this study, we demonstrated that AOH1996 caused oncogene-dependent cytotoxicity in both KRAS- and MYC-driven PDAC cells. Interestingly, BxPC3 cells (KRAS wild type) showed high sensitivity due to a BRAF-activating 15–base pair deletion at L485-P490 resulting in elevated TRCs.[7,41] Distinct from the reported therapeutic approaches for targeting TRCs that enhance transcriptional pausing, AOH1996 demonstrates a unique trapping mechanism that promotes TRCs by enhancing the interaction of RNAPII and PCNA.[15] Consistent with this trapping mechanism, we observed enhanced RNAPII-PCNA interaction in the PLA assay. Consequently, we note dose-dependent inhibition of replication fork progression due to AOH1996. Interestingly, inhibition of replication fork progression by AOH1996 was not associated with a significant compensatory increase in new origin firing, suggesting additional mechanisms of DNA replication inhibition that may impede replication licensing are at play. Although AOH1996 may cause DNA damage by interfering with multiple other PCNA-related processes, our findings suggest that most of the AOH1996-related DNA damage in PDAC cells is likely a consequence of TRCs. The study uncovers a previously uncharacterized role of AOH1996 in causing transcription shutdown through proteasome-mediated degradation of RNAPI and RNAPII. We speculate that AOH1996-mediated cancer cell death is realized through a combination of both TRC-induced DNA damage and transcription shutdown. Indeed, transcription inhibition through small molecule therapy (using triptolide) has previously been shown to be an effective strategy in PDAC models, albeit with high toxicity.[42] In contrast, the lack of toxicity with AOH1996 in our studies may be related to tumor-selective replication stress-dependent transcription inhibition. Further ongoing studies will likely delineate additional mechanisms for therapeutic efficacy of AOH1996.

In PDAC organoid models we found considerable heterogeneity of response to AOH1996. Organoid models have been increasingly used to model clinical responses more accurately than conventional 2-dimensional models.[23,43] For clinical translation, it is imperative to develop a biomarker of response to TRC-targeting approach. Dreyer et al[14] first characterized a replication stress signature that was particularly enriched in the basal subtype and did not overlap with DNA damage repair deficiency signature. Consistent with the observation of Dreyer et al,[14] we found partial overlap between basal and replication signatures. We discovered that TRC targeting was most effective in the 2 of 3 organoid lines exhibiting replication stress high transcriptomic signature. Because only 1 of the 3 sensitive lines had a strongly basal signature, we are unable to conclude if classical or basal subtype is a predictor of response to AOH1996. However, the activity of AOH1996 in a basal organoid line as well as Met-high KPCXY mouse cell

Figure 3. Impact of AOH1996 on TRCs in PDAC. (*A* and *B*) Flow cytometric RNAPII-PCNA PLA. Panc1 cells were treated without or without AOH1996 (as indicated) for 24 hours and the interaction between transcription machinery protein (RNAPII) and replication scaffold (PCNA) was quantified as a measure of TRCs using flow cytometric RNAPII-PCNA PLA assay. For this analysis, the threshold of high vs low TRCs was set at the median of control. Representative data (from 2 independent experiments) are shown in a stacked bar graph (*A*) and histogram (*B*) (****$P < .0001$, unpaired *t* test). At least 10,000 cells were quantified. (*C*) Immunocytometric RNAPII-PCNA PLA was performed in Panc1 cells. Cells were treated with increasing doses of AOH1996 (as indicated) for 24 hours. PLA was performed to quantify TRCs as mean fluorescence intensity per cell. Violin plot is demonstrated. One-way ANOVA with Tukey adjustment for multiple comparisons, ****$P < .0001$. (*D*) Immunocytochemistry for DNA damage marker (gH2AX) with or without 24-hour exposure to 500 nM AOH1996 or 500 nM gemcitabine or DMSO in MIA Paca-2 cells. Transcription inhibitor DRB (100 mM, last 2 hours) was used as indicated. The data points demonstrate an average of 3 to 4 independent experiments and error bars indicate standard deviation. Analysis shown is 1-way ANOVA with Sidak's multiple comparison test, comparing the indicated conditions (***$P = .0005$; ns, not significant). (*E*) Western blot: Indicated PDAC cells were treated with 500 nM AOH1996 for 14 hours. Proteasome inhibitor (MG132) was added for the last 2 hours. UV (30 J/m^2 over 30 minutes) was used as a positive control. Representative immunoblots of protein extracts from each pancreatic cancer cell line tested are shown. Actin was used as the loading control (RNAPIIo, elongating RNA Polymerase II; RNAPIIa, inactive RNA Polymerase II). (*F* and *G*) Global transcription was measured in MIA Paca-2 cells after exposure to AOH1996 500 nM or gemcitabine 500 nM for 12 hours. DRB is used as a positive control for transcription inhibition (100 mM, 2 hours). Violin plots depicting fluorescence intensity from a representative experiment are shown in (*F*) and images are shown in (*G*). Analysis shown is 1-way ANOVA with Dunnett multiple comparison test, comparing different conditions with DMSO control (****$P < .0001$, *0.012). DAPI, 4′,6-diamidino-2-phenylindole. Q8

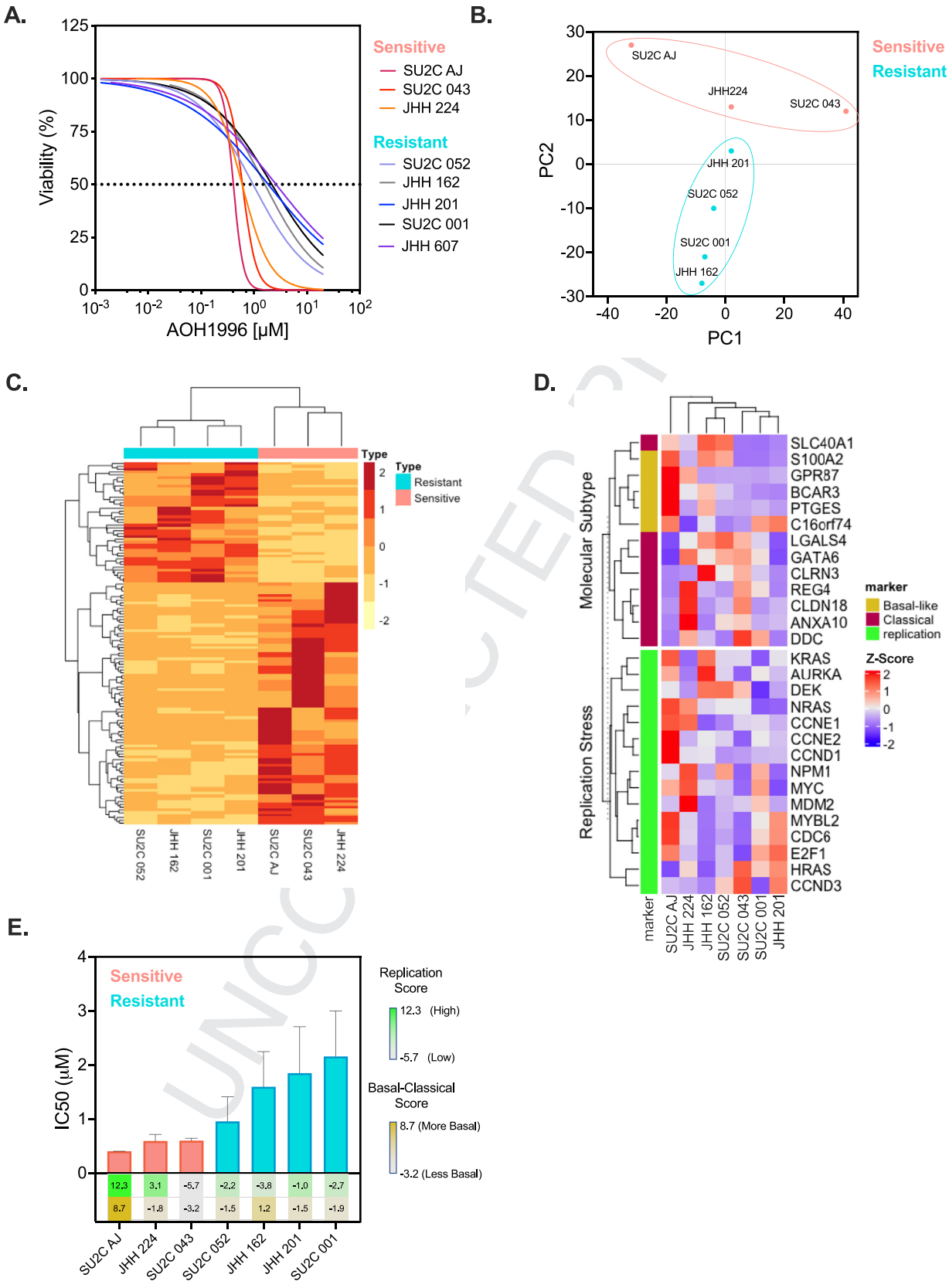

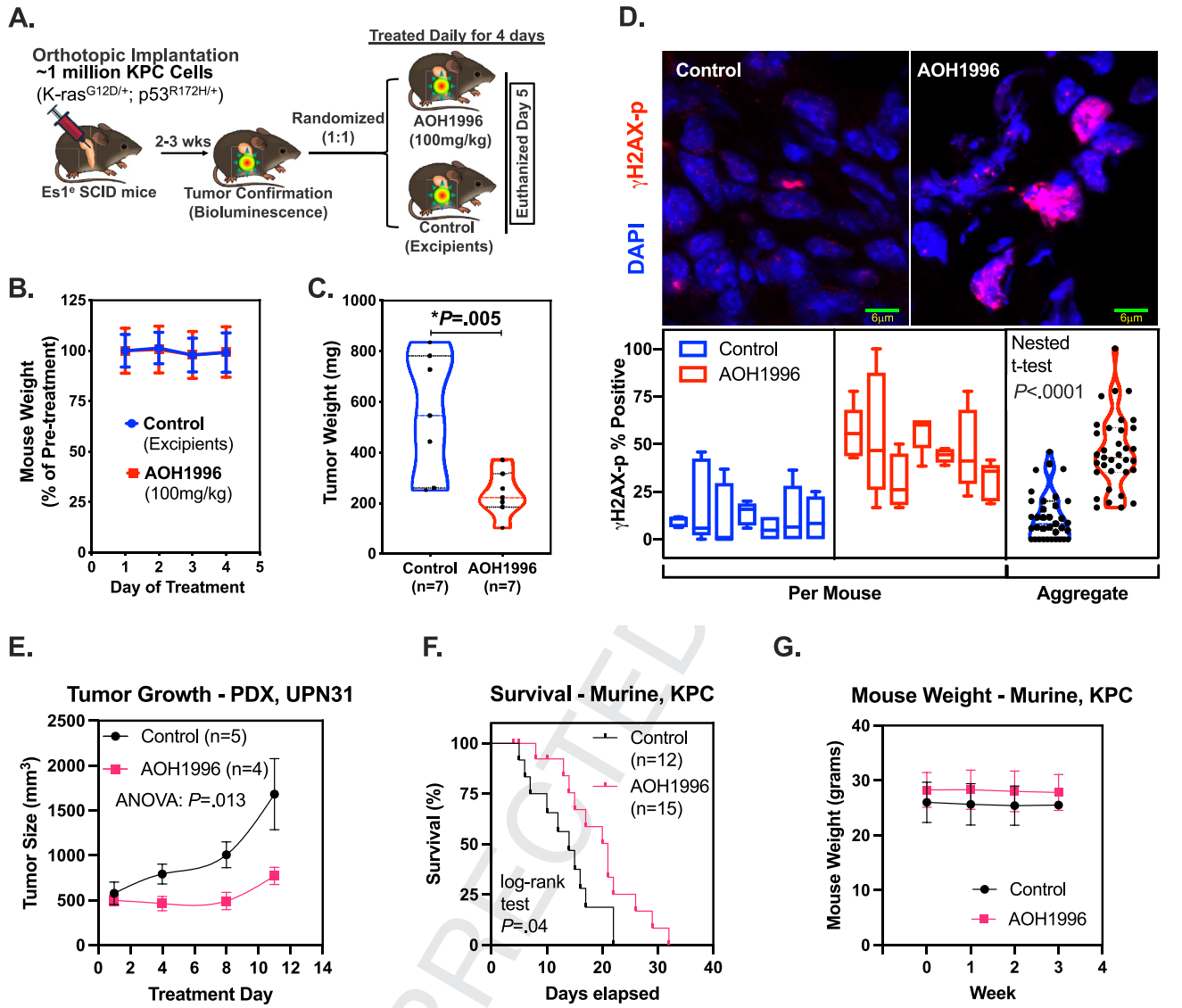

Figure 5. In vivo therapeutic efficacy of AOH1996 in PDAC. (*A*) Mouse model: Mouse pancreatic cancer (KPC) cell line was isolated from KPC (LSL-KrasG12D/+; LSL-Trp53R172H/+) mouse PDAC tumor and modified to express luciferase. KPC cells were orthotopically implanted in carboxyl esterase–deficient (ES1^{e}) SCID mice. Mice were then imaged using bioluminescence at 2 to 3 weeks after tumor cell implantation to confirm tumor formation and randomized to treatment with AOH1996 or control. Treatment was given for 4 days. Mice were euthanized on day 5. Mouse (*B*) and tumor (*C*) weights are shown (1-sided Mann-Whitney test, $P = .005$). See Supplementary Figures 4–6 for additional details. (*D*) Fluorescent immunostaining for DNA damage marker (gH2AXp) in fresh frozen sections of tumors treated with AOH1996 compared with controls from experiment (*A*) (Nested *t* test, $P < .0001$). At least 5 sections per mouse tumor and 100 cell nuclei were analyzed. (*E*) Ectopic patient-derived xenograft UPN31 implanted in the flank of carboxyl esterase–deficient ES1^{e} SCID mice were allowed to grow to approximately 500 mm^3 then randomized to receive AOH1996 (100 mg/kg) orally or excipients (control). Tumor volume was recorded. Mean and standard deviation are reported. (*F* and *G*) Survival experiment. Mice corresponding to the tumor model in (*A*) were randomized after tumor confirmation on bioluminescence and treated with AOH1996 (100 mg/kg, 5 days a week) or excipients (control) by oral gavage. Mice were euthanized when they met Institutional Animal Care and Use Committee–approved euthanasia criteria. Kaplan-Meier survival analysis is shown in (*F*) and tumor weights in (*G*).

Figure 4. AOH1996 targets replication stress high subtype of PDAC. (*A*) PDAC organoids from patient tumors were exposed to increasing concentrations (0–20 μM) of AOH1996 for 72 hours and then analyzed using the CellTiter-Glo assay. Cell viability is reported as % of control, with 100% representing a zero response. Lines indicate best-fit values derived from a log-inhibitor vs response model with variable slope using Prism. Sensitive and resistance cell lines were defined based on the hill slope parameter with sensitive cell lines demonstrating hill slope of < -1. (*B*) Principal component analysis derived from gene-expression data from the indicated organoid lines. PC1 and PC2 are shown, which described most of the variation in the data. (*C*) Heatmap of gene-expression profiles of sensitive and resistant organoid lines cluster distinctly; 130 top differentially expressed genes are shown. (*D*) Gene-expression signatures for PDAC subtypes are demonstrated for each sample. (*E*) IC50 values derived from the model in 4A are shown with replication stress and basal signature scores for DNA damage marker (gH2AX) with or without 24-hour exposure to 500 nM.

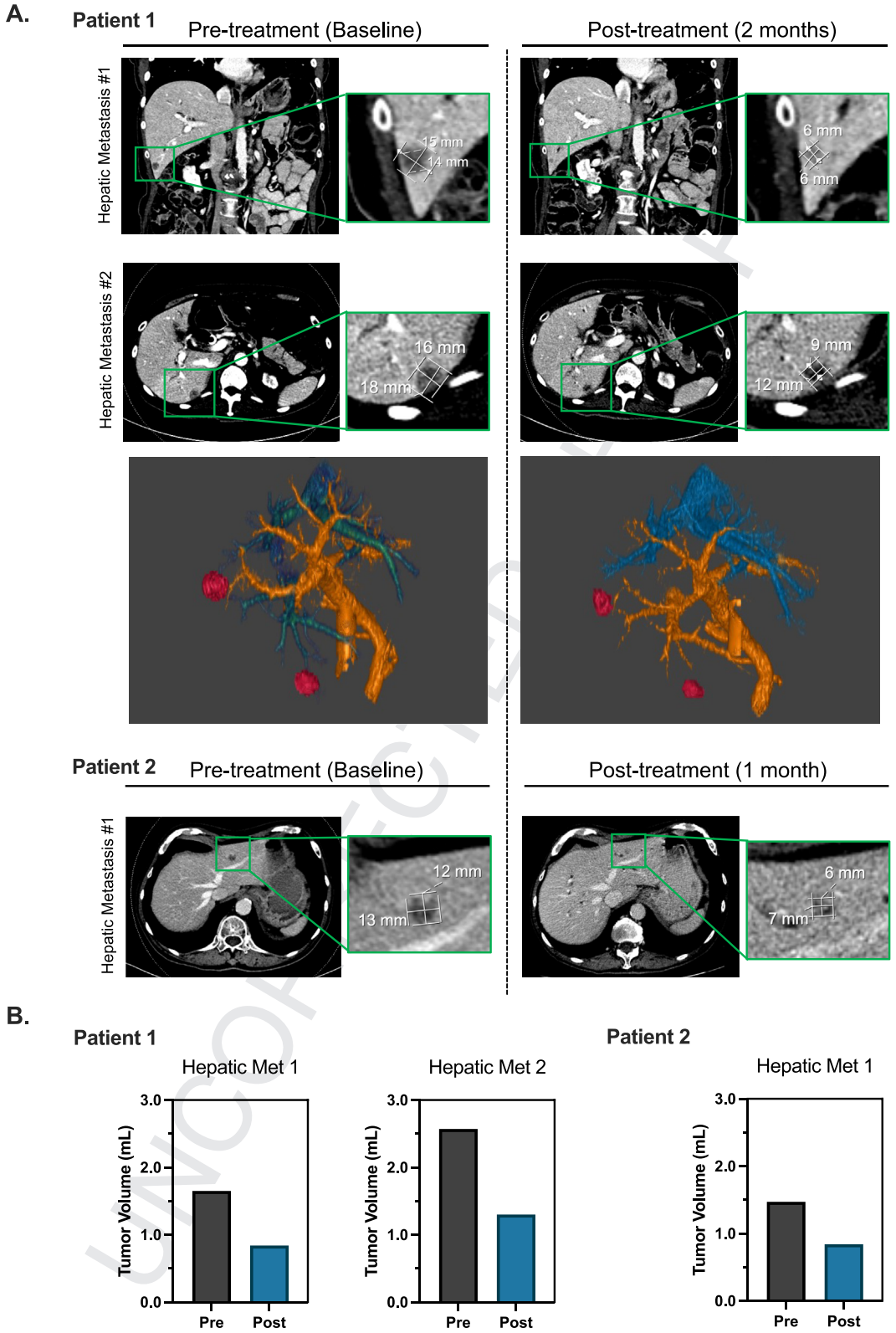

Figure 6. Axial and coronal images from CT scans pre- and posttreatment with AOH1996 from 2 patients with metastatic PDAC are shown along with 3-dimensional reconstruction (*A*) and tumor volume quantification (*B*).

lines (which exhibit basal signature[22]) is particularly relevant because basal subtype is an aggressive variant of PDAC with the worst prognosis and limited response to the most effective chemotherapy.[44] These observations provide a rationale for further evaluation of basal and replication stress high transcriptomic biomarkers as predictors of response to TRC-targeting therapies such as AOH1996 in the clinic.

Therapeutic responses in in vitro models were also recapitulated in the in vivo murine models. We noted a robust growth inhibition in both patient and mouse-derived models. In survival experiments, AOH1996 treatment prolonged survival but was not curative. Although these observations provide a strong rationale for further development of a TRC-targeting strategy for PDAC, they also highlight the limitation in using monotherapy for successful clinical translation. Consistent with prior observations in mice and dogs,[15] we found AOH1996 to be nontoxic in this study at effective doses. Notably, in this study, we provide first evidence of efficacy of a TRC-targeting approach in patients with metastatic PDAC, both of whom demonstrated shrinkage of hepatic tumors with AOH1996 monotherapy. However, we also noted heterogeneity of response with nonhepatic liver metastases being nonresponsive to therapy. However, due to unavailability of tumor tissue from liver metastases, we were unable to characterize the divergent responses observed by metastatic site. These early observations underscore the need not only to characterize optimal candidates for AOH1996 but also highlight the importance of studying the effect of AOH1996 in the context of the tumor microenvironment. Ongoing work is exploring rational combination therapies in combination with TRC targeting in PDAC.

Supplementary Material

Note: To access the supplementary material accompanying this article, visit the online version of *Gastroenterology* at www.gastrojournal.org, and at https://doi.org/10.1053/j.gastro.2025.02.038.

References

1. Kotsantis P, Petermann E, Boulton SJ. Mechanisms of oncogene-induced replication stress: jigsaw falling into place. Cancer Discov 2018;8:537–555.
2. Waters AM, Der CJ. KRAS: the critical driver and therapeutic target for pancreatic cancer. Cold Spring Harb Perspect Med 2018;8:a031435.
3. Kotsantis P, Silva LM, Irmscher S, et al. Increased global transcription activity as a mechanism of replication stress in cancer. Nat Commun 2016;7:13087.
4. Tuveson D. Abstract IA-10: Overcoming the seven deadly hallmarks of pancreatic cancer. Cancer Res 2020;80:IA-10.
5. Grabocka E, Commisso C, Bar-Sagi D. Molecular pathways: targeting the dependence of mutant RAS cancers on the DNA damage response. Clin Cancer Res 2015;21:1243–1247.
6. Bowry A, Kelly RDW, Petermann E. Hypertranscription and replication stress in cancer. Trends Cancer 2021;7:863–877.
7. Meng F, Li T, Singh AK, et al. Base-excision repair pathway regulates transcription-replication conflicts in pancreatic ductal adenocarcinoma. Cell Rep 2024;43:114820.
8. Laquente B, Lopez-Martin J, Richards D, et al. A phase II study to evaluate LY2603618 in combination with gemcitabine in pancreatic cancer patients. BMC Cancer 2017;17:137.
9. O'Connor MJ. Targeting the DNA damage response in cancer. Mol Cell 2015;60:547–560.
10. Holter S, Borgida A, Dodd A, et al. Germline BRCA mutations in a large clinic-based cohort of patients with pancreatic adenocarcinoma. J Clin Oncol Off J Am Soc Clin Oncol 2015;33:3124–3129.
11. Golan T, Hammel P, Reni M, et al. Overall survival from the phase 3 POLO trial: maintenance olaparib for germline BRCA-mutated metastatic pancreatic cancer. J Clin Oncol 2021;39:378; 378.
12. Golan T, Hammel P, Reni M, et al. Maintenance olaparib for germline BRCA-mutated metastatic pancreatic cancer. N Engl J Med 2019;381:317–327.
13. Rahib L, Smith BD, Aizenberg R, et al. Projecting cancer incidence and deaths to 2030: the unexpected burden of thyroid, liver, and pancreas cancers in the United States. Cancer Res 2014;74:2913–2921.
14. Dreyer SB, Upstill-Goddard R, Paulus-Hock V, et al. Targeting DNA damage response and replication stress in pancreatic cancer. Gastroenterology 2021;160:362–377.e13.
15. Gu L, Li M, Li CM, et al. Small molecule targeting of transcription-replication conflict for selective chemotherapy. Cell Chem Biol 2023;30:1235–1247.e6.
16. Paunesku T, Mittal S, Protić M, et al. Proliferating cell nuclear antigen (PCNA): ringmaster of the genome. Int J Radiat Biol 2001;77:1007–1021.
17. Smith SJ, Li CM, Lingeman RG, et al. Molecular targeting of cancer-associated PCNA interactions in pancreatic ductal adenocarcinoma using a cell-penetrating peptide. Mol Ther Oncolytics 2020;17:250–256.
18. Yue H, Na Y-L, Feng X-L, et al. Expression of p57kip2, Rb protein and PCNA and their relationships with clinicopathology in human pancreatic cancer. World J Gastroenterol 2003;9:377–380.
19. Wang S-C. PCNA: a silent housekeeper or a potential therapeutic target? Trends Pharmacol Sci 2014;35:178–186.
20. Manuel ER, Chen J, D'Apuzzo M, et al. Salmonella-based therapy targeting indoleamine 2,3-dioxygenase coupled with enzymatic depletion of tumor hyaluronan induces complete regression of aggressive pancreatic tumors. Cancer Immunol Res 2015;3:1096–1107.
21. Ying H, Kimmelman AC, Lyssiotis CA, et al. Oncogenic Kras maintains pancreatic tumors through regulation of anabolic glucose metabolism. Cell 2012;149:656–670.
22. Maddipati R, Norgard RJ, Baslan T, et al. MYC levels regulate metastatic heterogeneity in pancreatic adenocarcinoma. Cancer Discov 2022;12:542–561.
23. Seppälä TT, Zimmerman JW, Sereni E, et al. Patient-derived organoid pharmacotyping is a clinically tractable strategy for precision medicine in pancreatic cancer. Ann Surg 2020;272:427–435.
24. Sebaugh JL. Guidelines for accurate EC50/IC50 estimation. Pharm Stat 2011;10:128–134.
25. Frum RA, Deb S, Deb SP. Use of the DNA fiber spreading technique to detect the effects of mutant p53 on DNA replication. Methods Mol Biol 2013;962:147–155.
26. Raoof M, Zhu C, Cisneros BT, et al. Hyperthermia inhibits recombination repair of gemcitabine-stalled replication forks. J Natl Cancer Inst 2014;106:dju183.
27. Jao CY, Salic A. Exploring RNA transcription and turnover in vivo by using click chemistry. Proc Natl Acad Sci U S A 2008;105:15779–15784.

28. Raoof M, Cisneros BT, Corr SJ, et al. Tumor selective hyperthermia induced by short-wave capacitively-coupled RF electric-fields. PLoS One 2013;8:e68506.
29. Campbell PM, Groehler AL, Lee KM, et al. K-Ras promotes growth transformation and invasion of immortalized human pancreatic cells by Raf and phosphatidylinositol 3-kinase signaling. Cancer Res 2007;67:2098–2106.
30. Weibrecht I, Leuchowius K-J, Clausson C-M, et al. Proximity ligation assays: a recent addition to the proteomics toolbox. Expert Rev Proteomics 2010;7:401–409.
31. Li M, Xu X, Chang C-W, et al. SUMO2 conjugation of PCNA facilitates chromatin remodeling to resolve transcription-replication conflicts. Nat Commun 2018;9:2706.
32. Gómez-González B, Aguilera A. Transcription-mediated replication hindrance: a major driver of genome instability. Genes Dev 2019;33:1008–1026.
33. Juiz N, Elkaoutari A, Bigonnet M, et al. Basal-like and classical cells coexist in pancreatic cancer revealed by single-cell analysis on biopsy-derived pancreatic cancer organoids from the classical subtype. FASEB J 2020;34:12214–12228.
34. Negrini S, Gorgoulis VG, Halazonetis TD. Genomic instability—an evolving hallmark of cancer. Nat Rev Mol Cell Biol 2010;11:220–228.
35. Bryant KL, Mancias JD, Kimmelman AC, et al. KRAS: feeding pancreatic cancer proliferation. Trends Biochem Sci 2014;39:91–100.
36. Hamperl S, Bocek MJ, Saldivar JC, et al. Transcription-replication conflict orientation modulates R-loop levels and activates distinct DNA damage responses. Cell 2017;170:774–786.e19.
37. Stork CT, Bocek M, Crossley MP, et al. Co-transcriptional R-loops are the main cause of estrogen-induced DNA damage. eLife 2016;5:e17548.
38. Bowry A, Piberger AL, Rojas P, et al. BET inhibition induces HEXIM1- and RAD51-dependent conflicts between transcription and replication. Cell Rep 2018;25:2061–2069.e4.
39. Roeschert I, Poon E, Henssen AG, et al. Combined inhibition of Aurora-A and ATR kinase results in regression of MYCN-amplified neuroblastoma. Nat Cancer 2021;2:312–326.
40. Patel PS, Algouneh A, Krishnan R, et al. Excessive transcription-replication conflicts are a vulnerability of BRCA1-mutant cancers. Nucleic Acids Res 2023;51:4341–4362.
41. Vaseva AV, Blake DR, Gilbert TSK, et al. KRAS suppression-induced degradation of MYC is antagonized by a MEK5-ERK5 compensatory mechanism. Cancer Cell 2018;34:807–822.e7.
42. Vispé S, DeVries L, Créancier L, et al. Triptolide is an inhibitor of RNA polymerase I and II–dependent transcription leading predominantly to down-regulation of short-lived mRNA. Mol Cancer Ther 2009;8:2780–2790.
43. Seppälä TT, Zimmerman JW, Suri R, et al. Precision medicine in pancreatic cancer: patient-derived organoid pharmacotyping is a predictive biomarker of clinical treatment response. Clin Cancer Res 2022;28:3296–3307.
44. Aung KL, Fischer SE, Denroche RE, et al. Genomics-driven precision medicine for advanced pancreatic cancer: early results from the COMPASS trial. Clin Cancer Res 2018;24:1344–1354.

Received January 17, 2024. Accepted February 25, 2025.

Correspondence
Address correspondence to: Mustafa Raoof, MD, Department of Surgery, Cancer Genetics and Epigenetics, City of Hope National Medical Center, MALP 2229, 1500 East Duarte Road, Duarte, California 91010. e-mail: mraoof@coh.org. Q2

Acknowledgments
Shanna J. Smith, Fan Meng, and Robert G. Lingeman contributed equally. Q6

Research reported in this publication included work performed in the following: Shared resources supported by the National Cancer Institute of the National Institutes of Health under grant number P30CA033572: Q12 Analytical Cytometry; Light Microscopy & Digital Imaging; Integrative Genomics; Small Animal Imaging; and Research Histology. The content is solely the responsibility of the authors and does not necessarily represent the official views of the National Institutes of Health. This work was funded in part by the National Comprehensive Cancer Network (NCCN) Foundation. Any opinions, findings, and conclusions expressed in this material are those of the author(s) and do not necessarily reflect those of NCCN or the NCCN Foundation. We are grateful to the patients who participated in the clinical trial.

CRediT Authorship Contributions
Shanna J. Smith, PhD (Conceptualization: Equal; Data curation: Equal; Formal analysis: Equal; Investigation: Equal; Writing – original draft: Equal; Writing – review & editing: Equal)

Fan Meng, PhD (Conceptualization: Equal; Data curation: Equal; Formal analysis: Equal; Investigation: Equal; Writing – original draft: Equal)

Robert G. Lingeman, BS (Conceptualization: Equal; Data curation: Equal; Formal analysis: Equal; Investigation: Equal; Writing – original draft: Equal)

Caroline M. Li, PhD (Data curation: Supporting; Investigation: Supporting; Writing original draft: Supporting)

Min Li, PhD (Data curation: Supporting; Investigation: Supporting; Methodology: Supporting)

Galyah Boneh, MS (Data curation: Supporting; Writing – review & editing: Supporting)

Toni T. Seppälä, PhD (Data curation: Supporting; Formal analysis: Supporting; Investigation: Supporting; Writing – review & editing: Supporting)

Thuy Phan, PhD (Data curation: Supporting; Writing – review & editing: Supporting)

Haiqing Li, PhD (Formal analysis: Equal; Methodology: Equal; Writing – review & editing: Supporting)

Richard A. Burkhart, MD, PhD (Data curation: Supporting; Formal analysis: Supporting; Resources: Supporting; Supervision: Supporting; Writing – review & editing: Supporting)

Vishwas Parekh, MD, PhD (Data curation: Supporting; Formal analysis: Supporting; Writing – review & editing: Supporting)

Syed Rahmanuddin, MD (Formal analysis: Supporting; Writing – review & editing: Supporting)

Laleh G. Melstrom, MD (Conceptualization: Supporting; Resources: Supporting; Writing – review & editing: Supporting)

Robert J. Hickey, PhD (Resources: Supporting; Writing – review & editing: Supporting)

Vincent Chung, MD (Investigation: Supporting; Resources: Supporting; Writing review & editing: Supporting)

Yilun Liu, PhD (Investigation: Supporting; Supervision: Supporting; Writing – review & editing: Supporting)

Linda H. Malkas, PhD (Resources: Supporting; Writing – review & editing: Supporting)

Mustafa Raoof, MD, MS (Conceptualization: Lead; Data curation: Lead; Formal analysis: Lead; Funding acquisition: Lead; Investigation: Lead; Methodology: Lead; Project administration: Lead; Resources: Lead; Software: Lead; Supervision: Lead; Validation: Lead; Visualization: Lead; Writing – original draft: Lead; Writing – review & editing: Lead)

Conflict of interests
These authors disclose the following: City of Hope's Office of Technology Licensing has been awarded a patent on AOH1996. Linda H. Malkas and Robert J. Hickey are listed as inventors. The remaining authors disclose no conflicts. Q3

Funding
The work performed in this study was supported by the following funding sources awarded to Mustafa Raoof: Pancreatic Cancer Action Network Career Development Award (grant no. 20-20-RAOO), National Comprehensive Cancer Network Young Investigator Award (grant no. P062683), American Cancer Society: IRG (grant no. 132966-IRG), American College of Surgeons Faculty Research Fellowship, City of Hope Academic Innovation Fund, anonymous philanthropic support (GK & KK), and BG Family. Q4

Data Availability
The data supporting the findings of this study are available on reasonable request to the senior authors. Q5

Supplementary Methods

Cell Culture Conditions

MIA PaCa-2, PANC-1, KPC, and UPN3 cell lines were cultured in Dulbecco's modified Eagle's medium (DMEM) (Mediatech), supplemented with 10% fetal bovine serum (FBS) and 1% penicillin/streptomycin (P/S). Capan-1 cell lines were cultured in Iscove's modified Dulbecco's medium (IMDM) (Mediatech), supplemented with 20% FBS and 1% P/S. Capan-1 C2-14 cell line was a generous gift from Prof Toshiyasu Taniguchi.[e1] BxPC-3 cell lines were cultured in RPMI-1640 (Mediatech), supplemented with 10% FBS and 1% P/S. All cell cultures were maintained at 37°C in 5% CO_2. HPNE, KPCXY cells, and iKRAS cells and their culture conditions have been described previously. iKRAS cell lines were a generous gift from Prof Haoqiang Ying.[e2] Murine KPCXY cell lines were a generous gift from Dr Ravikanth Maddipati.[e3] All cells used in these studies were verified to be mycoplasma free within 6 months of the experiments. Organoid cell lines were generated from untreated patient resected tumors or biopsies as described previously.[e4]

DNA Fiber Analysis

DNA fiber assays were performed using a modified version of the technique described by Frum et al.[e5] In brief, actively dividing MIA PaCa-2 cells (500,000 cells/well of a 6-well dish) were pulse-labeled with 100 μM of chlorodeoxyuridine (CldU) (Sigma-Aldrich) for 15 minutes at 37°C and 5% CO_2 in complete media. The CldU was subsequently removed from the cells by washing 3 times with 1x phosphate-buffered saline (PBS) (Corning). The cells were then pulse-labeled with 200 μM iododeoxyuridine (IdU) (Sigma-Aldrich) for 30 minutes in the presence of 0, 0.5 μM, 1 μM, or 2 μM AOH1996 at 37°C, 5% CO_2 for 30 minutes. After labeling, the cells were washed 3 times with PBS and collected by trypsinization and centrifugation at 500*g* for 5 minutes. The pelleted cells were resuspended in PBS and counted with a Beckman Coulter Z2 particle counter. Two thousand cells were spread on a microscope slide (Leica) and lysed by layering lysis buffer (0.5% sodium dodecyl sulfate [SDS], 200 mM Tris-HCL pH 7.4, 400 mM NaCl, 0.2% NP40) on the cells. The slides were placed at an angle (15°–45°) to allow the DNA fibers to spread down the slides. Four replicate slides were made for each experimental condition. The slides were then fixed with 3:1 methanol/acetic acid and the DNA denatured with 2.5 M HCl. Following a blocking step, the DNA fibers were hybridized with an antibody specific to CldU (Abcam) that was derived from rat, and an antibody specific to IdU (BD Biosciences) that was derived from mouse. The primary antibodies were then detected using secondary antibodies conjugated to a fluorophore: goat anti-rat immunoglobulin (Ig)G conjugated to AlexaFluor 488 (Thermo Fisher Scientific) and rabbit anti-mouse IgG conjugated to AlexaFluor 594 (Thermo Fisher Scientific). After washing, coverslips were mounted onto slides and DNA fibers were imaged using the fluorescent setting of the Zeiss Observer II (Carl Zeiss AG) widefield light microscope at ×100 magnification. In post-processing, Image J (National Institutes of Health) was used to visualize and measure green and red fluorescing lengths of DNA fibers. The fibers chosen for measurement were those with a clearly defined section of a green fluorescence followed immediately by a section of red fluorescence, and only fibers with similar lengths of green fluorescence (as judged typical for the experiment) were scored.

Western Blot Analysis

Western blot analysis was performed as previously described.[e6] Cells were seeded in 100 mm tissue culture–treated culture dishes, grown to approximately 75% confluency, and treated with 200 nM AOH 1996. Treatment was stopped at specified time points (4, 24, and 48 hours), and cells were washed 3 times in ice cold TBS (20 mM Tris, pH 7.6, and 137 mM NaCl). The cells were then harvested into TBS, 2x Thermo Scientific Halt phosphatase inhibitor cocktail, 2x Halt protease inhibitor cocktail (Thermo Fisher Scientific), and 10 mM EDTA. Harvested cells were pelleted in a swinging bucket centrifuge at 1500 rpm for 5 minutes, the supernatant was removed, and the pellets were stored at −80 °C before processing. Thawed pellets were then sonicated in SDS buffer (100 mM Tris, pH 6.8, 4% SDS, 20% glycerol, 1x Thermo Scientific Halt phosphatase inhibitor cocktail, 1x Halt protease inhibitor cocktail, and 5 mM EDTA) at 30% amplitude in 10-second intervals until no longer viscous. After heating at 95 °C for 5 minutes and cooled, the total protein concentration was determined by DC Protein Assay (Bio-Rad). DTT and bromophenol blue were added to a final concentration of 90 mM DTT and ∼0.08% bromophenol blue, respectively. After resolving the protein extract by SDS–polyacrylamide gel electrophoresis, it was transferred to nitrocellulose membrane using the Pierce G2 Fast Blotter (Thermo Fisher Scientific) and total protein loading was visualized using Ponceau-S staining solution (Sigma-Aldrich). The blots were blocked in 5% nonfat dried milk and 0.05% tween 20 for 1 hour. Antibodies recognizing H2AX (Cell Signaling Technology), phospho-histone H2AX Ser139 (Millipore), RNAPII (A10, Santa Cruz Biotech), and actin (Abcam) were detected by ECL prime and imaged on the Azure c600 (Azure Biosystems).

Immunocytochemistry Staining of γH2AX

Immunocytochemistry was performed as described previously.[e7] Circular #1.5 cover slips (Electron Microscopy Sciences) were placed in 12-well plates and sterilized by UV exposure for 20 minutes. Approximately 15,000 exponentially growing MIA PaCa-2 cells were seeded in each well, and adherent sub-confluent monolayers were observed growing on the cover slip 24 hours later. Cells were then exposed to various treatment conditions, as described in the Results section. After treatment, cells were fixed in 1% paraformaldehyde in PBS (wt/vol) for 30 minutes, permeabilized using 0.3 % (vol/vol) Triton-100 and 0.125% (wt/vol) CHAPS (3-[(3-Cholamidopropyl) dimethylammonio]-1-propanesulfonate) dissolved in PBS for 15 minutes, blocked for 1 hour in a 3% (wt/vol) bovine serum albumin

(BSA) and 1% (vol/vol) normal goat serum, labeled with γ-H2AX mouse monoclonal primary antibody (Millipore), followed by secondary labeling with Alexa Fluor 647-conjugated goat anti-mouse antibody. At the end of immunolabeling, 4',6-diamidino-2-phenylindole (DAPI) (Millipore) was used to counter stain DNA at 0.1 μg/mL for 15 minutes. Between each step, cells were washed with PBS 3 times for 5 minutes each time on a leveled shaker at 50 rpm. Cover slips were washed one more time with PBS and were mounted on frosted glass slides (Thermo Fisher Scientific) using Dako mounting media (Dako). The slides were sealed with a conventional nail polish hardener and stored at 4°C until imaging.

Immunocytochemistry for Nucleolin

For correlation studies between nucleolin and gH2AX, MIA PaCa2 cells were seeded on collagen-coated slides on 6-well plates. After reaching 40% to 50% confluence, the cells were treated with 500 nM AOH1996 and gemcitabine, respectively, for 12 hours. The treated cells were fixed with 4% paraformaldehyde (PFA) for 15 minutes at room temperature, sequentially washed with DPBS twice, and permeabilized with 0.5% NP40 on ice for 5 minutes. The cells were then washed with DPBS thrice and then blocked with 2% BSA-DPBS buffer at room temperature for 1 hour, followed by overnight incubation at 4°C with 1:500 diluted gH2AX (Millipore 05-636-I) and nucleolin (CST 14574T) antibodies. After labeling with primary antibodies, the cells were washed 3 times with DPBS and incubated with Alex Flour 488 anti-Rabbit (Invitrogen A11008) and Texas Red anti-mouse (Invitrogen T862) secondary antibodies for 1 hour at room temperature under dark conditions. The cells were then stained with DAPI for 15 minutes before mounting and image acquisition. Images were acquired using ZEISS LSM900 confocal light microscopy, and then processed with ZESIS ZEN Blue to calculate the Pearson's correlation coefficient of gH2ax (red) and nucleolin (green) signal per cell. The coefficient was plotted and analyzed using GraphPad Prism 10.30.

Confocal Imaging

For confocal imaging, a Zeiss LSM 700 confocal microscope was used. Images were acquired using an LCI Plan Neofluar 63x/1.3 Water Imm Corr M27 objective for a 1024 × 1024-pixel array at 0.05 μm/pixel. Samples were excited using a solid-state laser at 405 nm (768 gain) for DAPI, 639 nm (901 gain for the first biological replicate and 777 gain for the second biological replicate) for Alexa Fluor 647. Exposure settings were set to maximize dynamic range initially and then kept constant across multiple samples to allow quantitative comparisons. Acquired images were processed in Image Pro Premier (version 9.2, Media Cybernetics, Inc). Nuclei were identified using the DAPI channel. For counting γ-H2AX foci, as there was background signal for the Alexa Fluor 647 signal, the images from the control condition (DMSO treatment) were used to determine a threshold for the Alexa Fluor 647 signal, defining the threshold such that fewer than 10% of cells in the control condition were counted as positive for γ-H2AX foci, and signals that appeared to be adjacent foci were counted as individual foci rather than counting 2 foci as 1. Positive cells were defined as those having 5 or more γ-H2AX foci in the nucleus. For each biological replicate, the threshold was determined using the control condition within that replicate, and this threshold was applied to all images acquired as part of that replicate; for the first biological replicate, the Alexa Fluor 647 signal intensity threshold was set to the range 58 to 255 (arbitrary units); for the second biological replicate, the threshold was set to the range 98 to 255 (arbitrary units). For foci segmentation purposes, Smoothing was set to 1, and Grow was set to −1, and Watershed splitting was applied during foci counting. Approximately 100 cells per condition per experiment were counted.

Cell Proliferation Assay Using Flow Cytometry

MIA PaCa-2 cells (either untreated or treated with 200 nM AOH 1996) were pulse-labeled with 10 μM of bromodeoxyuridine (BrdU) in DMEM supplemented with 10% FBS and 1% P/S for 1 hour at 37°C. Pulse-labeled cells were then recovered, washed, and processed for BrdU staining using the protocol specified in the BD Pharmingen BrdU Flow Kit (BD Life Sciences). Briefly, the cells were fixed, permeabilized, stained with anti-BrdU, and counterstained with fluorescein isothiocyanate-conjugated (FITC) goat anti-mouse IgG1. Following 7-aminoactinomycin D (7-AAD) staining, cellular data were acquired using the BD FACSDiva software with the BD LSRFORTESSA. Offline analysis was performed using FlowJo v10 software.

Cell Proliferation With Real-Time Cell Analysis

For measuring the differential AOH1996 inhibitory effect on KRAS(G12D)-expressing cells, the real-time cell analysis (RTCA) assay was used to measure real-time cell growth. The HPNE-KRAS(G12D) cells were pretreated with or without 2 ng/mL doxycycline for 72 hours until 60% to 70% confluency; 4000 cells were then seeded on an E-plate (Agilent 05469830001). Cell growth curves were recorded on xCELLigence RTCA DP (Agilent) at 15-minute intervals under standard cell culture conditions (37°C, 5% CO_2). AOH1996 was added 40 hours after cells seeding at indicated concentrations.

Cytofluorometric Analysis of Nuclear Apoptosis by TUNEL Assay

Nuclear apoptosis was assessed by the TUNEL assay. This assay was performed using the In Situ Cell Death Detection Kit, TMR red kit (Roche) according to the manufacturer's protocol. Briefly, PBS-washed MIA PaCa-2 cells (2×10^7 cells/mL) were fixed with 2% paraformaldehyde (MilliporeSigma) for 60 minutes at 15 to 25°C. Fixed cells were washed twice in PBS and permeabilized using 0.1% Triton X-100 in 0.1% sodium citrate for 2 minutes on ice. After another PBS wash step, cells were incubated with 50 μL of TUNEL reaction mixture for 1 hour at 37°C in a dark, humidified atmosphere. TdT enzyme was not added for the

negative control. Cells were washed twice more in PBS before analysis. Cellular data were acquired using the BD FACSDiva software with the BD LSRFORTESSA. Offline analysis was performed using FlowJo v10 software.

Proximity Ligation Assay for TRC Determination

To quantify TRCs, we performed proximity ligation assay (PLA) as described previously.[e8] Briefly, treated cells at 60% to 70% confluence were trypsinized, washed at least 1 time with DPBS, then fixed with 4% PFA for 15 minutes followed by permeabilization with 5-minute incubation with 0.5% NP-40. The fixed cell pellets were then collected after centrifugation at 400*g* for 5 minutes and washed with DPBS twice, blocked with commercial block buffer (supplied in kit) at room temperature for 1 hour, and then incubated with RNAPII-CTD S2 (1:100) and PCNA (1:100) antibody overnight in 4°C. PLA reactions were performed using the manufacturer's supplied instructions in the kit (Sigma-Aldrich). PLA-fluorescent labeled cells were passed through a 100-μm strainer, and the PLA signal was measured using Attune NXT cytometer. FlowJo was used for data processing, analysis, and visualization.

Global RNA Transcription Quantification

Global RNA quantification was performed using the Click-iT RNA Alexa Fluor 488 Imaging Kit (Thermo Fisher Scientific) according to manufacturer-supplied methodology and as reported previously.[e9] Briefly, pancreatic cancer cells were plated at 40% confluence and allowed to attach overnight. The cells were then treated with indicated conditions for 48 hours. Subsequently, all cells were treated with 1 mM 5-ethynyl uridine final concentration for 1 hour. Cell fixation, permeabilization, and Click-iT Detection were performed per protocol.

RNA-Sequencing Analysis

RNA sequencing (RNA-seq) was performed as described previously.[e10] The RNA-seq datasets are merged based on the Hg38 gene symbols. The extremely low expressed genes and the genes that were not detected in all datasets were filtered out. R-package ComBat-seq was used to remove the batch effects.[e11] Differential gene expression analysis was performed on the batch effect–corrected RNA-seq expression data using R-package DESeq2 version 1.26.0.[e12] The top differentially expressed genes between drug-resistant samples and drug-sensitive samples were selected using adjusted P value $<.05$. The heatmap of differentially expressed genes was generated using R-package pheatmap (version 1.0.12). The principal component analysis plot, the volcano plot, and dot plot are generated using R-package ggplot2 (version 3.4). Basal and Classical classification and scoring were based on signatures that have been reported previously.[e13] Replication stress signature and scoring were generated based on a previous report.[e14] The replication stress score of each cell line is the sum of the Z-score normalized RNA-seq expression of published replication stress marker genes.

Mouse Models of Pancreatic Cancer

An orthotopic PDAC model was generated, as described previously.[e15,e16] Approximately 1 million (1×10^6) luciferase-expressing KPC cells in 10 mL volume were injected in the pancreas of a carboxyl esterase-deficient ES1^e/SCID mouse using a 30-gauge-needle tip (point style 4; Hamilton Company). The KPC cell line was isolated from KPC (LSL-KrasG12D/+; LSL-Trp53R172H/+) mice that are known to recapitulate human pancreatic cancer. Tumor growth was monitored via bioluminescence imaging using a Lago scanner (Spectral Instruments Imaging Inc). Once tumors were confirmed (at approximately 2–3 weeks), mice were enrolled in the study, and treatments were assigned.

An ectopic patient-derived xenograft model was developed from a resected patient tumor that was passaged subcutaneously in immune-deficient NSG mice. Tumors from donor mice were harvested when they reached 1.5 cm in size. A 4-mm^2 tumor fragment was placed in the recipient mice subcutaneously in the flank. Upon engraftment, mice were then randomized to AOH1996 or excipient groups.

After completion of treatment, mice were euthanized via carbon dioxide inhalation, and tumor weights were measured. All animals were handled, housed, and studied in accordance with a protocol (Institutional Animal Care and Use Committee #18026) that was reviewed and approved by the City of Hope Institutional Animal Care and Use Committee. Office of Laboratory Animal Welfare, National Institutes of Health, US Department of Health and Human Services guidelines were followed as well.

Immunohistochemistry

Immunohistochemistry (IHC) was performed on Ventana Discovery Ultra IHC autostainer (Ventana Medical Systems) using the ChromoMap DAB detection system according to the manufacturer's recommendations. Briefly, tissue samples were sectioned at a thickness of 5 μm and put on positively charged glass slides. Deparaffinization, rehydration, endogenous eroxidase activity inhibition and Q7 antigen retrieval were all performed on the automated stainer. Slides were then incubated with either primary rabbit anti-K67 monoclonal antibody (Ventana), or rabbit anti-H2AX monoclonal antibody (Abcam), followed by DISCOVERY anti-rabbit HQ and DISCOVERY anti-HQ-horseradish peroxidase, visualized with ChromoMap DAB detection Kit (Ventana). The slides were then counterstained with hematoxylin (Ventana) and coverslipped.

TUNEL on Mouse Tissues

To determine apoptosis, TUNEL method was performed by using The ApopTag Peroxidase In Situ Apoptosis Detection Kit (Millipore) based on the manufacturer's instructions. Briefly, sections were deparaffinized and washed in PBS, followed by proteinase K pretreatment and endogenous peroxidase activity quenching. Labeling was performed by adding TdT enzyme mix to the tissue sections and the reaction was stopped by immersing slides in stop buffer followed by 3 PBS washes. After adding anti-digoxigenin conjugate to the slide; the color was

developed by Peroxidase Substrate Kit diaminobenzidine (DAB) (Vector Laboratories, Inc.). Finally, the slides were counterstained with hematoxylin (Ventana) and coverslipped.

Image Acquisition and Quantification for IHC

All glass slides were digitized in a Ventana iScan HT (Roche-Ventana Medical Systems) at a magnification of ×40. Quantification profiles of the digitized whole slides were performed using QuPath software.[e17] Quantification of the positive cells with the Ki67 and TUNEL stains was carried out with the positive cell detection function. To avoid selection bias and increase statistical accuracy, the entire tissue section was manually selected using the polygon tool taking care to exclude areas rich in immune and stromal cells. The software performed annotation and quantification and expressed the positive cell counts as a percentage of positive cells detected per total cells.

Fluorescence Immunohistochemistry

For fluorescence immunohistochemistry, frozen tissues embedded in optimal cutting temperature compound were sectioned at 5 μm and fixed on glass slides using acetone. Staining was performed similarly to immunocytochemistry. Confocal imaging was performed with a confocal microscope (Zeiss LSM 700) and analyzed using Image Pro Premier (version 9.3, Media Cybernetics, Inc.).

Bioluminescence Imaging

Two to 3 weeks after implantation of tumor cells in the pancreas, bioluminescence measurements were performed to confirm the presence of tumor in the pancreas. D-Luciferin from firefly (Gold Biotechnology) was administered intraperitoneally at a dose of 200 μg in 200 μL PBS. Animals were anesthetized using 2% isoflurane and imaged using a Lago scanner (Spectral Instruments Imaging Inc.) 10 to 12 minutes after the injection. The imaging was performed with an exposure time of 10 seconds with 2-fold binning, a 1.2 f/stop, and a 25-cm field of view. Mice that had any bioluminescence activity above background (suggesting the development of tumors) were included in the study.

Treatment Assignment and Administration

Mice with confirmed tumors based on bioluminescence were then randomized into 2 groups, either treatment with AOH1996 or treatment with vehicle control using the Random.org List Randomizer (https://www.random.org/lists/). Randomization was blinded as the tumors were not visible to the naked eye and the investigator performing the randomization was separate from the investigator administering treatments.

Mice with tumors were treated once per day for 4 days with either 100 mg/kg AOH1996 or vehicle control via oral gavage. The formulation was previously described (Gu et al., 2018); this formulation allowed for a concentration of AOH1996 at 22.6 mg/g. The formulation was mixed at 60% with sterilized ultrapure water (40%) and sonicated until homogeneous; this step was performed immediately before treatment. After 4 days of treatment, mice were euthanized using dual method. Necropsy was performed and tumor masses were measured. Tumors, normal pancreas, spleen, lung, heart, intestine, kidney, and livers were harvested for downstream studies.

Image Acquisition

Contrast CT of the chest, abdomen, and pelvis was performed from the lung apices through the pelvis. Images of the abdomen were obtained before and after the administration 125 mL Isovue-370 contrast. Postcontrast images of the chest and pelvis were obtained. Oral contrast was administered. Coronal and sagittal reformatted images were obtained. Up-to-date CT equipment and radiation dose reduction techniques were used (CTDIvol: 5.9–6.1 mGy, DLP: 341 mGy-cm).

Initial images were reconstructed into 0.625 × 1.25-mm slices for 3-dimensional (3D) post-processing and uploaded from the picture archiving and communication system to advanced imaging software (Vitrea Advanced Visualization 7.15.2) for volumetric analysis.

3D Volumetric Measurement

Contrast CT images of the abdomen were transferred into Food and Drug Administration–approved Vital Images advanced imaging workstation (Vitrea Advanced Visualization 7.15.2). All thin reconstructed images were uploaded into the 3D workstation. The liver and both tumor volumes were extracted with the automated mode or by drawing the region of interest around the tumor. The portal vein, hepatic vein, and hepatic artery segmentation were performed using the automated tool. All 2D images were then edited with the manual tool (as required on each slice) on specific slices and analyzed for liver and liver tumor volume quantification. Changes in the volume will be assessed by using the density-based voxel quantification, which includes liver volume, tumor volume, average, minimum, and maximum in the Hounsfield unit. All the numbers are saved in Excel file for the purpose of statistical analysis.

Supplementary Results

■■■

Supplementary References

e1. Sakai W, Swisher EM, Karlan BY, et al. Secondary mutations as a mechanism of cisplatin resistance in BRCA2-mutated cancers. Nature 2008;451:1116–1120.

e2. Ying H, Kimmelman AC, Lyssiotis CA, et al. Oncogenic Kras maintains pancreatic tumors through regulation of anabolic glucose metabolism. Cell 2012;149:656–670.

e3. Maddipati R, Norgard RJ, Baslan T, et al. MYC levels regulate metastatic heterogeneity in pancreatic adenocarcinoma. Cancer Discovery 2022;12:542–561.

e4. Seppälä TT, Zimmerman JW, Suri R, et al. Precision medicine in pancreatic cancer: patient-derived organoid

pharmacotyping is a predictive biomarker of clinical treatment response. Clin Cancer Res 2022;28:3296–3307.

e5. Frum RA, Deb S, Deb SP. Use of the DNA fiber spreading technique to detect the effects of mutant p53 on DNA replication. Methods Mol Biol 2013;962:147–155.

e6. Smith SJ, Li CM, Lingeman RG, et al. Molecular targeting of cancer-associated PCNA interactions in pancreatic ductal adenocarcinoma using a cell-penetrating peptide. Mol Ther Oncolytics 2020;17:250–256.

e7. Raoof M, Zhu C, Cisneros BT, et al. Hyperthermia inhibits recombination repair of gemcitabine-stalled replication forks. J Natl Cancer Inst 2014;106:dju183.

e8. Meng F, Singh A, Li T, et al. Base excision repair pathway regulates transcription-replication conflicts in pancreatic ductal adenocarcinoma. MS ID#: BIORXIV/2023/560510.

e9. Jao CY, Salic A. Exploring RNA transcription and turnover in vivo by using click chemistry. Proc Natl Acad Sci U S A 2008;105:15779–15784.

e10. Seppälä TT, Zimmerman JW, Sereni E, et al. Patient-derived organoid pharmacotyping is a clinically tractable strategy for precision medicine in pancreatic cancer. Ann Surg 2020;272:427–435.

e11. Zhang Y, Parmigiani G, Johnson WE. ComBat-seq: batch effect adjustment for RNA-seq count data. NAR Genom Bioinform 2020;2:lqaa078.

e12. Love MI, Huber W, Anders S. Moderated estimation of fold change and dispersion for RNA-seq data with DESeq2. Genome Biology 2014;15:550.

e13. Juiz N, Elkaoutari A, Bigonnet M, et al. Basal-like and classical cells coexist in pancreatic cancer revealed by single-cell analysis on biopsy-derived pancreatic cancer organoids from the classical subtype. FASEB J 2020; 34:12214–12228.

e14. Dreyer SB, Upstill-Goddard R, Paulus-Hock V, et al. Targeting DNA damage response and replication stress in pancreatic cancer. Gastroenterology 2021; 160:362–377.e13.

e15. Manuel ER, Chen J, D'Apuzzo M, et al. Salmonella-based therapy targeting indoleamine 2,3-dioxygenase coupled with enzymatic depletion of tumor hyaluronan induces complete regression of aggressive pancreatic tumors. Cancer Immunol Res 2015; 3:1096–1107.

e16. Raoof M, Cisneros BT, Corr SJ, et al. Tumor selective hyperthermia induced by short-wave capacitively-coupled RF electric-fields. PLoS One 2013;8: e68506.

e17. Bankhead P, Loughrey MB, Fernández JA, et al. QuPath: open source software for digital pathology image analysis. Sci Rep 2017;7:16878.

A.

Pairwise Comparisons between IC50 generated from Figure 1D

	IC50 (nM)	MiaPaca-2	Panc1	BxPC3	Capan-1	KPC
MiaPaca-2	210	NA	F 109.10 (P<0.0001)	F 69.08 (P<0.0001)	F 19.54 (P<0.0001)	F 19.79 (<0.0001)
Panc1	2520	F 109.10 (P<0.0001)	NA	F 145.8 (P<0.0001)	F 39.09 (P<0.0001)	F 2.31 (P=0.1330)
BxPC3	33	F 69.08 (P<0.0001)	F 145.8 (P<0.0001)	NA	F 82.04 (P<0.0001)	F 56.99 (P<0.0001)
Capan-1	589	F 19.54 (P<0.0001)	F 39.09 (P<0.0001)	F 82.04 (P<0.0001)	NA	F 4.33 (P=0.0395)
KPC	1282	F 19.79 (<0.0001)	F 2.31 (P=0.1330)	F 56.99 (P<0.0001)	F 4.33 (P=0.0395)	NA

B.

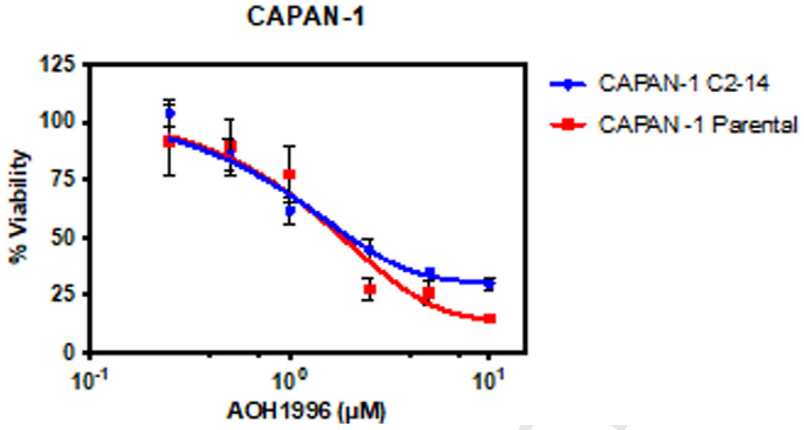

Supplementary Figure 1. (*A*) Comparison of IC50 values. Data shown in Figure 1*D*. To compare IC50 values we asked if the best-fit-values of IC50 defer between cell lines. Pairwise comparison of IC50 values was performed using extra sum-of-squares F-test. (*B*) Effect of AOH1996 on human CAPAN-1 viability using CellTiter Glo Assay Parental CAPAN-1 cells harbor pathogenic BRCA2 mutation (BRCA2.6174delT) that leads to homologous recombination repair deficiency, whereas C2-14 clone has a BRCA2 reversion that restores homologous recombination repair. AOH1996 demonstrated similar efficacy against the 2 cell lines. A representative experiment is shown with each datapoint representing mean of 4 to 6 observations and error bars indicating standard deviation. The line indicates nonlinear best-fit values.

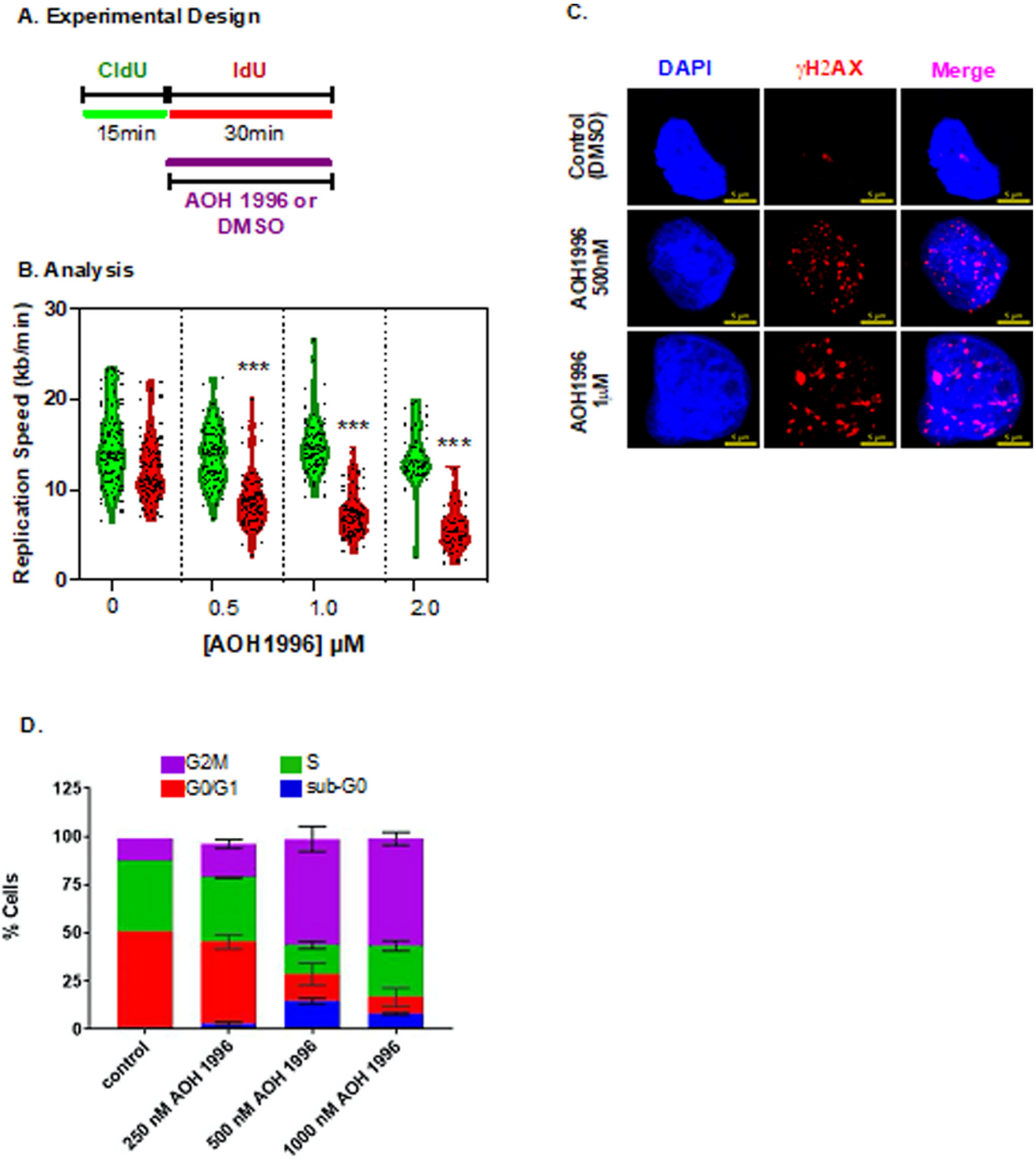

Supplementary Figure 2. Effect of AOH1996 on DNA replication in pancreatic cancer cells. (*A*) Experimental design. DNA fiber analysis was performed. Replicating DNA was labeled with CldU for 15 minutes, followed by IdU for 30 minutes. AOH 1996 or DMSO was added with IdU labeling. (*B*) Analysis: CldU and IdU tract lengths were measured (in microns) at each concentration of AOH1996 and were normalized to label exposure time to calculate replication speed. (1 micron = 2.59 kilobases). One-way ANOVA demonstrated significant decrease in replication speed during AOH1996 exposure (***$P < .0001$ for Dunnett multiple comparison test. Comparison performed with Red Violin Plot at 0 μM). (*C*) Immunocytochemistry: Representative images for DNA damage marker (gH2AX) for the experiment shown in Figure 2*E*. (*D*) Flow cytometry analysis similar to experiment shown in Figure 2*F* and *G*. The dose dependence of cycle changes was recorded after 24 hours of AOH1996 exposure, and then analyzed in triplicate. Average proportions are plotted in stacked bar graph with error bars indicating standard deviation.

web 4C/FPO

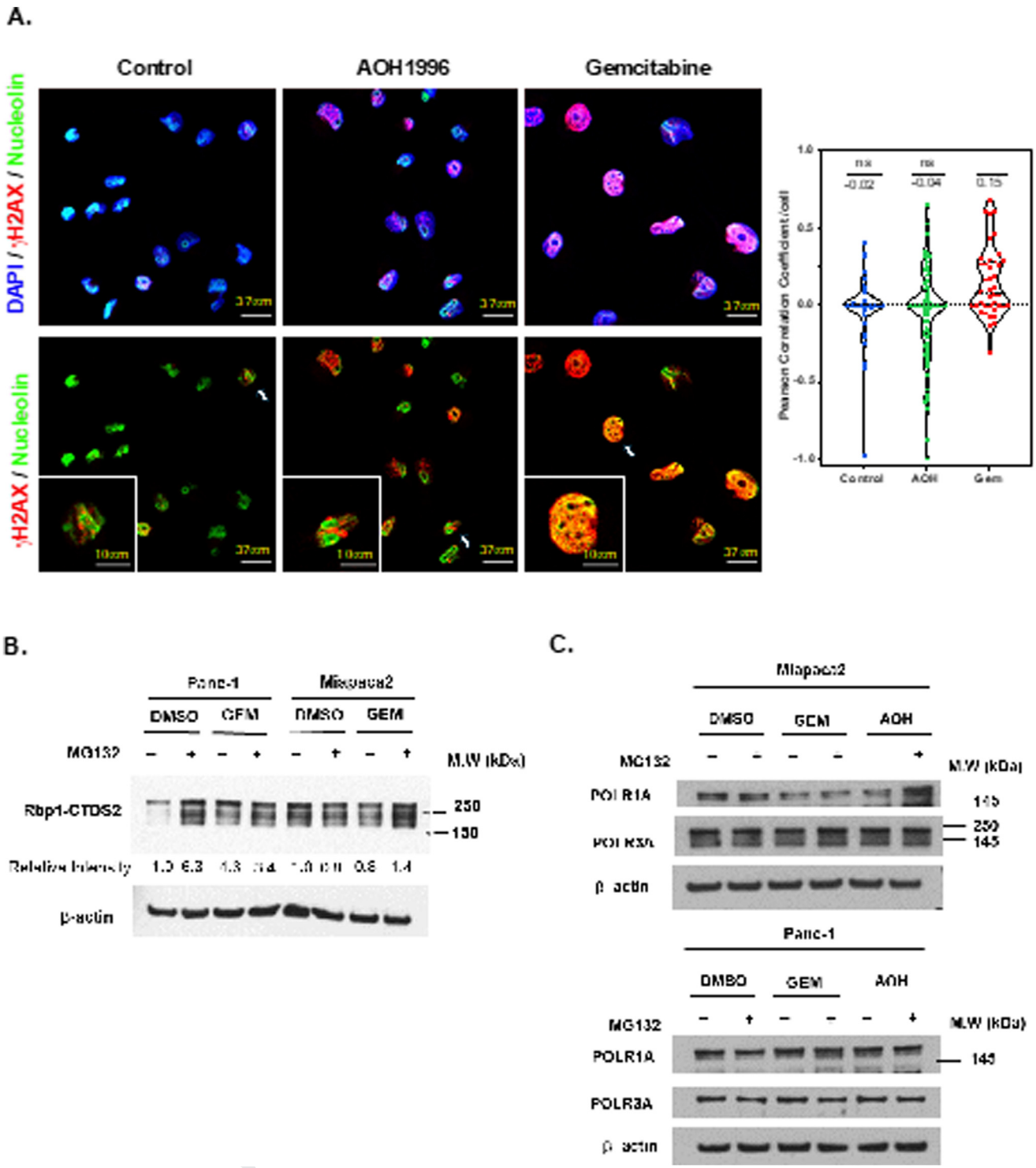

Supplementary Figure 3. (*A*) Immunocytochemistry: Colocalization of nucleolin and gH2AXp. MIA PaCa2 cells were treated with conditions depicted in Figure 3*D*. Pearson correlation coefficient was calculated to quantify the degreed of colocalization (0 = none, 1= perfect colocalization). (*B*) Western blot: Indicated PDAC cells were treated with 500 nM gemcitabine (GEM) or DMSO (Control) for 14 hours. Proteosome inhibitor (MG132) was added for the last 2 hours. Representative immunoblots of protein extracts from each pancreatic cancer cell line tested are shown. Actin was used as the loading control (RNAPII-CTDS2 = elongating RNA Polymerase II). (*C*) Western blot: Indicated PDAC cells were treated with gemcitabine (500 nM) or AOH1996 (500 nM) or DMSO (Control) for 14 hours. Proteosome inhibitor (MG132) was added for the last 2 hours. Representative immunoblots of protein extracts from each pancreatic cancer cell line tested are shown. Actin was used as the loading control (POLR1A = RNA Polymerase I, POLR3A = RNA Polymerase III).

web 4C/FPO

A.

Organoid Line	Source	Pre-treatment	Mutations	KRAS mutation
SU2C AJ	Biopsy	No	KRAS, TP53	G12C
SU2C 043	Biopsy	No	KRAS, TP53, CDKN2A, CTNNB1	G12V
JHH 224	Surgical	No	KRAS, BRCA1	G12D
SU2C 052	Biopsy	No	KRAS, BRCA2	G12V
JHH 162	Surgical	No	KRAS, TP53, SMAD4	G12R
JHH201	Surgical	Yes*	KRAS, TP53	G12D
SU2C 001	Biopsy	No	KRAS, SMAD4	G12D
JHH607	Surgical	No	KRAS, BRCA2, CDKN2A	G12D

*J1568 (Cyclophosphamide + Nivolumab + Urelumab + GVAX)

B.

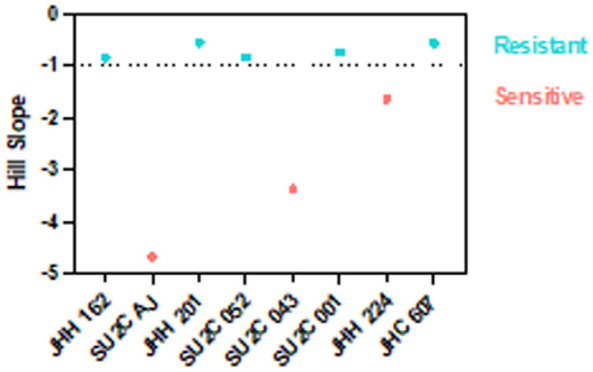

C.

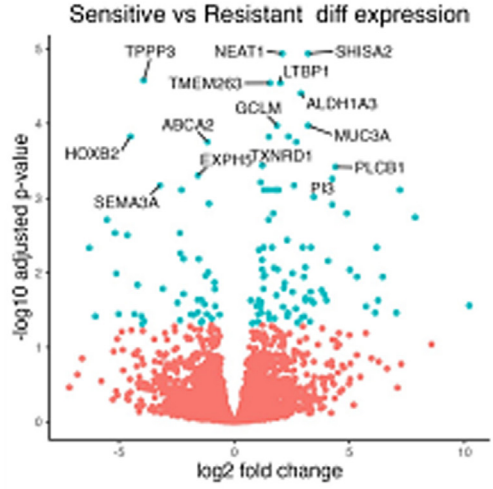

web 4C/FPO

Supplementary Figure 4. (*A*) Characteristics of PDAC organoid lines used for experiments shown in Figure 4. (*B*) Hill slope. The plot demonstrates hill slope value from dose-response curve shown in Figure 4*A*. Two distinct patterns of organoid cell death were apparent in the data. An abrupt decline in viability with increasing AOH1996 concentration vs a more gradual decline in viability. Therefore, the sensitivity threshold was defined based on the hill slope parameter. The resistant organoids had hill slope greater than −1 whereas sensitive organoids had hill slope less than −1. (*C*) Volcano plot demonstrating differential gene expression between resistant and sensitive organoid lines. The plot highlights the genes that are significantly differentially expressed in blue (adjusted *P* value < .05). The top 20 differentially expressed genes based on the adjusted *P* value are labeled.

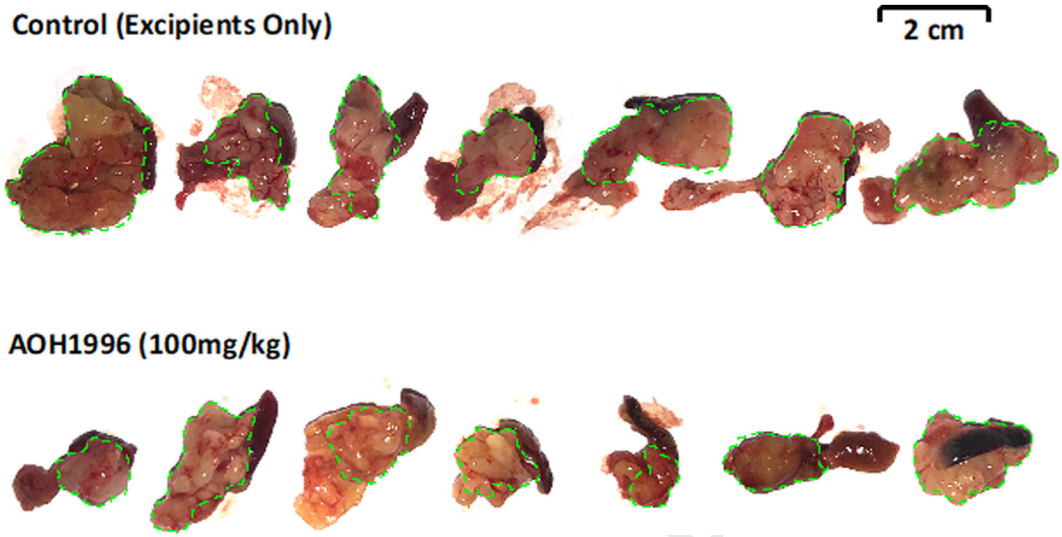

Supplementary Figure 5. Photograph of pancreatic tumors harvested from experimental mice (Figure 5*A*). Green outline identifies the area of the tumor.

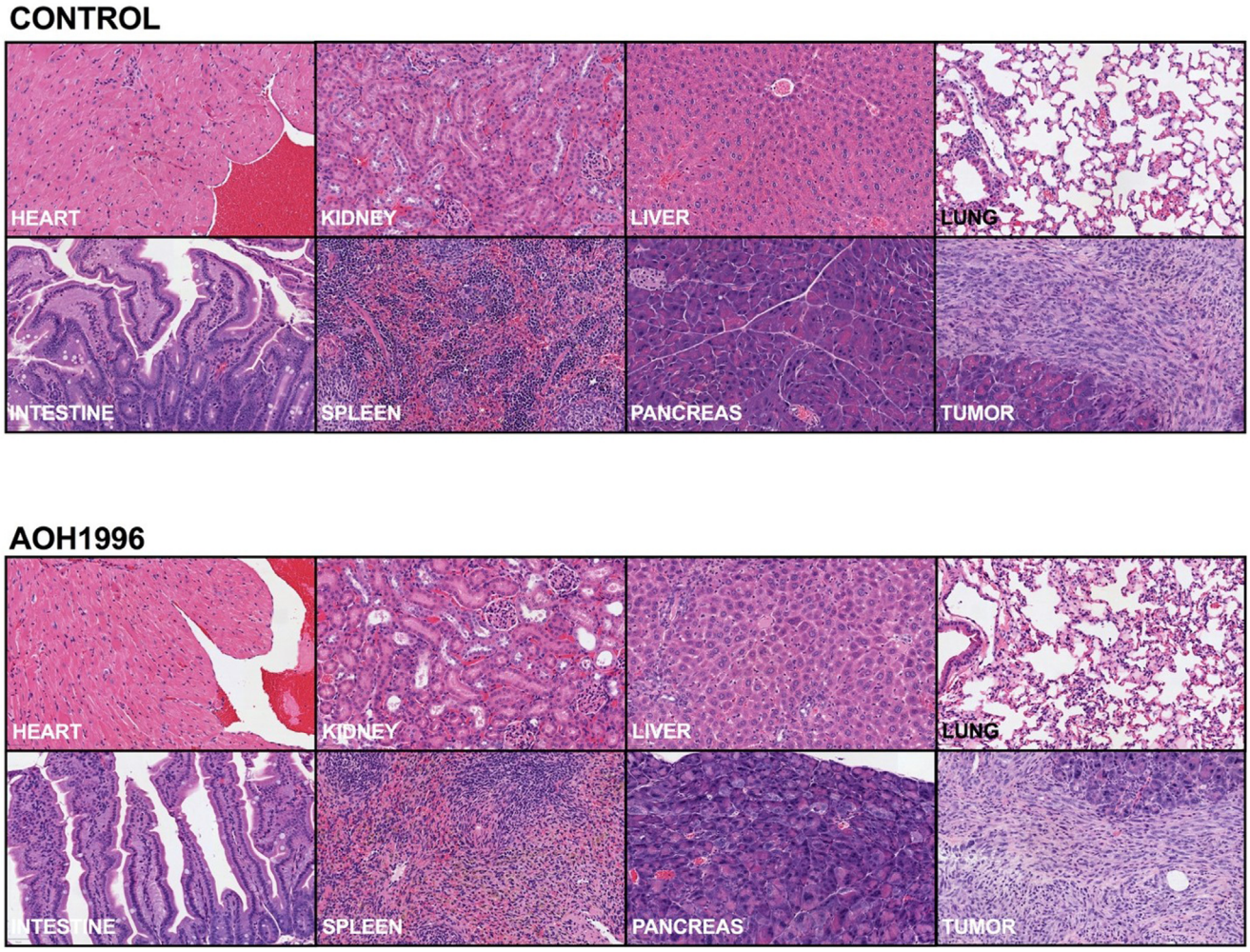

Supplementary Figure 6. Representative hematoxylin-eosin images from tumor and normal tissues from the control group vs AOH1996-treated mice. No toxicity was observed on histologic analysis.

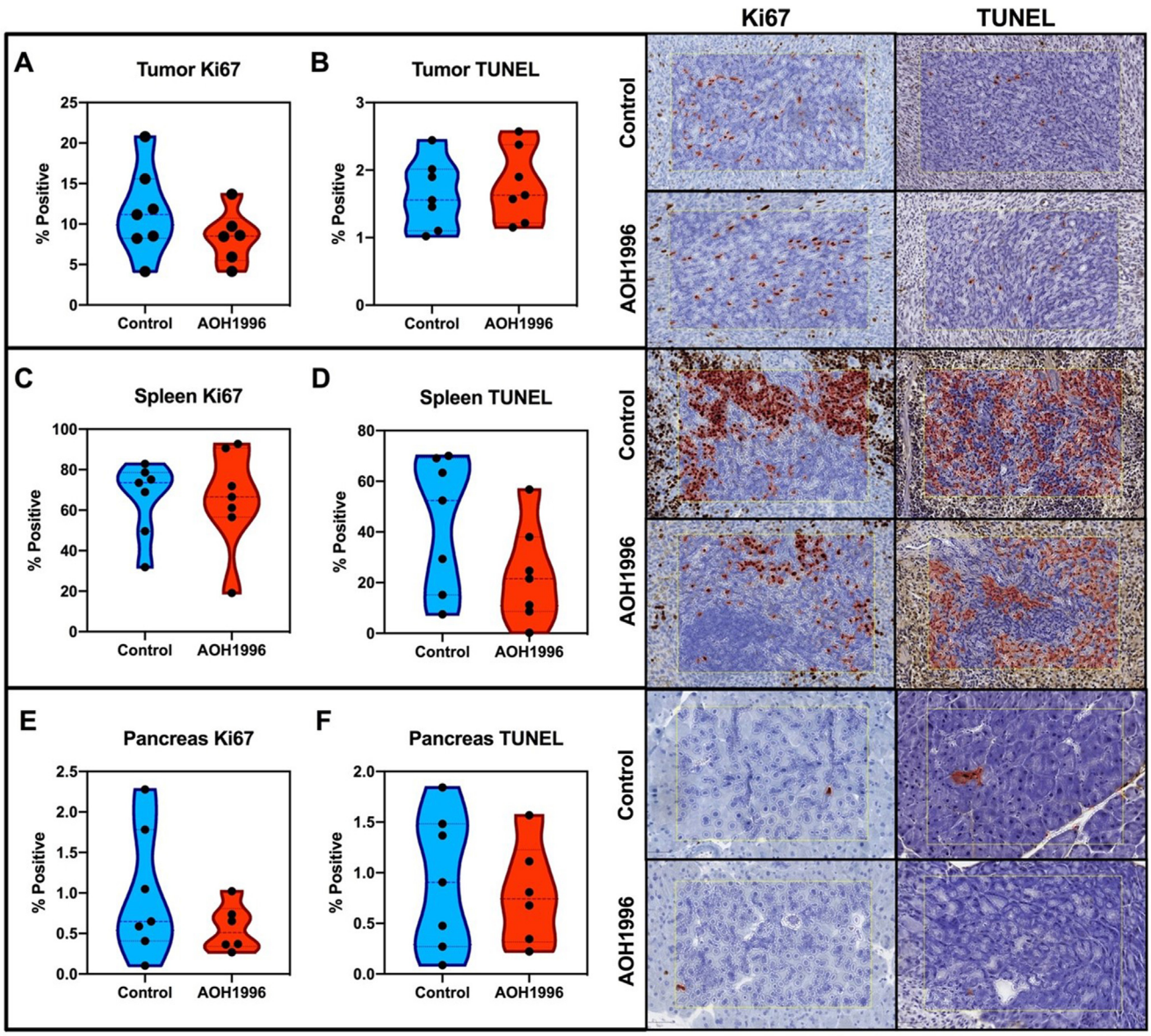

Supplementary Figure 7. Immunohistochemistry in mouse tumors and normal tissues. There were minimal changes in proliferation index (determined by Ki67) and apoptosis (determined by TUNEL staining) of mouse tumor and normal tissues. These changes were not statistically significant (*t* test, $P > .05$ for all comparisons). Q11

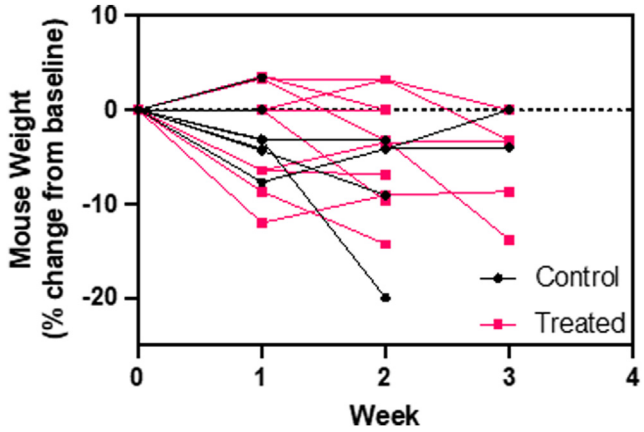

web 4C/FPO

Supplementary Figure 8. Individual mouse weights taken during the experiment in Figure 5*G*.